

## A MORPHOLOGY REVALUATION OF GALAXIES IN COMMON FROM THE CATALOG OF ISOLATED GALAXIES AND THE SLOAN DIGITAL SKY SURVEY (DR6)

H. M. HERNÁNDEZ-TOLEDO<sup>1</sup>, J. A. VÁZQUEZ-MATA<sup>2</sup>, L. A. MARTÍNEZ-VÁZQUEZ, V. AVILA-REESE,  
H. MÉNDEZ-HERNÁNDEZ, S. ORTEGA-ESBRÍ, J. P. MIRANDA-NÚÑEZ  
Instituto de Astronomía, Universidad Nacional Autónoma de México, A.P. 70-264, 04510 México D. F., México.  
*To appear in the Astronomical Journal*

### ABSTRACT

We present a revaluation of the optical morphology for 549 galaxies from the Catalog of Isolated Galaxies in the Northern Hemisphere (CIG; Karachentseva 1973) that are available in the Sloan Digital Sky Survey (SDSS; DR6). Both the high resolution and high dynamic range of the SDSS images and our semi-automatic image processing scheme, allow for a major quality and uniform morphological analysis. The processing scheme includes (1) sky-subtracted, cleaned, and logarithmic scaled  $g$ -band images; (2) filtered-enhanced versions of the images in (1); and (3) the corresponding RGB images available in the SDSS database. Special attention was paid for distinguishing between E, S0, and Sa candidates through an additional analysis of (4) the surface brightness,  $\epsilon$ ,  $PA$  and  $A_4/B_4$  Fourier series expansion profiles. An atlas of mosaics containing [(1), (2) and (3)] images for Sab-Sm/Irr types and [(1), (2), (3), (4)] images for E/S0/Sa types was produced and is available on the web. The median type in the sample corresponds to Sbc, with 65% of the sample being of this type or later. A scarce population of E (3.5%) and S0 (5%) galaxies amounting to 8.5%, and a non-negligible 14% fraction of early-type SaSab spirals are identified. We compare our results against a previous reclassification of the CIG catalog based on the digitized POSS II images (Sulentic et al. 2006). We calculate also the  $gri$  absolute magnitudes corrected by Galactic and internal extinctions and present the  $g-i$  color distribution and the color-magnitude diagram. Among the spirals, we find tentative fractions of strong and suspected bars of 65.8% and of 33.3% of rings. A detailed image analysis of the E galaxies (18) allows us to find a richness of distinct substructure in their isophotal shape and also of morphological distortions. At least 78% of the E galaxies show some kind of morphological distortion (shells, dust lanes, diffuse halos, etc.), suggesting that these galaxies suffered late dry mergers. The isophotes of 42% (37%) of the E galaxies are boxy (disky). Among 4 blue E's, 3 are disky. Finally, we calculate for all the sample the  $CAS$  (concentration, asymmetry and clumpiness) structural parameters in the  $ugriz$  bands. We analyze the loci of these galaxies in different projections of the  $CAS$  volume diagram and discuss some trends of the  $CAS$  parameters with the color band, as well as with the morphological type and the galaxy color.

*Subject headings:* Galaxies: spiral – Galaxies: irregulars – Galaxies: elliptical – Galaxies: lenticular – Galaxies: structure – Galaxies: photometry – Galaxies: fundamental parameters – Galaxies: morphology –

### 1. INTRODUCTION

A galaxy is considered as isolated if it has not suffered any interaction with another normal galaxy or with a group/cluster environment over a Hubble time or at least since approximately one half of its mass was assembled. In this sense, isolation offers a unique opportunity to identify the intrinsic physical and evolutive processes of galaxies, and then to confront the results with theoretical predictions of galaxy evolution (e.g., Avila-Reese et al. 2008). Isolated galaxies are also important as comparison objects in studies of the morphological mix as a function of environment, and the environmental effects on galaxy properties. However, the definition of isolated galaxy from an observational point of view is not an easy task. Karachentseva (1973) introduced an operational criterion for this definition and constructed the Catalog of Isolated Galaxies in the Northern Hemisphere (hereafter CIG), one of the most extended and used samples for these objects. The sample contains 1050 galaxies of

all morphological types and  $m_B < 15.7$  mag, identified in the photographic Palomar Observatory Sky Survey (POSS) plates. A careful revision of the morphology and general properties of these galaxies in the light of recent, much more detailed observations is highly desirable.

A first step in this direction has been given by Sulentic et al. (2006; hereafter Sul06), who revisited the morphology of the CIG galaxies by using the digitalized POSS II data, and found some fraction of galaxies having a morphological type different to those reported in the original CIG. In this paper, we are aimed to analyze the CIG galaxies in common with the huge galaxy sample of the Sloan Digital Sky Survey (SDSS), a sample that we will call  $CIG \cap SDSS$ . The advantages of the SDSS CCD images over previous image surveys in similar regions of the sky are notorious. Among these we mention: (1) the uniformity in both the instrumental set and photometric conditions, (2) the homogeneity in multicolor  $ugriz$  imaging and photometry, and (3) the high resolution (0.4 "/pix) of the images. These advantages are crucial for studying galaxy morphology and structural properties.

Because of the SDSS large numbers, uniformity, and

<sup>1</sup> E-mail: hector@astroscu.unam.mx

<sup>2</sup> E-mail: jvazquez@astroscu.unam.mx

completeness down to a certain magnitude, it is an ideal database for the search of fundamental relations between physical properties of galaxies and their dependencies on local and larger-scale environments. For example, recently Park et al. (2007,2008) used the SDSS data for studying the environmental dependence of the observed morphology –and other properties– at different density smoothing scales. Based on their results, they concluded that galaxy morphology depends primarily on the small scale environment, which may reflect the influence of later evolutionary effects such as galaxy–galaxy interactions, rather than on large-scale environment in which the galaxy initially formed. A relevant goal of the present paper is the identification of the isolated galaxies that may show evidence of morphological disturbances. It is possible that the isolated galaxies showing signs of distortions are the recent merger products, at a given large-scale background density, as predicted by Park, Gott & Choi (2008).

An important question concerning morphological classification is the correct definition of what is an elliptical (E), lenticular (S0) or early-type spiral (Sa) galaxy. These types are the most affected in their definition by saturation, poor resolution, etc. Saucedo–Morales & Biegging (2001) estimated that one–half of E galaxies could be misclassified in the POSS plates–based CIG catalog. The existence of true isolated early-type galaxies is in general an important problem in galaxy formation. Our finding of detailed structure in the E and S0 isolated galaxies is expected to provide new tests for the various hypotheses of their formation. Have the isolated E galaxies systematic differences from those ones found in groups and clusters? Have they assembled in the same way in both cases? Similar questions could be asked about the isolated S0 galaxies, whose detailed formation histories are poorly understood. A few decades back, Gott & Thuan (1976) argued that E galaxies were produced by larger initial–density fluctuations, which would have higher density at turnaround and where star formation (SF) would be completed before collapse. Such larger initial–density fluctuations would be more likely in a region that would later turn into a high density environment. In the modern context of the  $\Lambda$  Cold Dark Matter ( $\Lambda$ CDM) hierarchical model, the formation of E/S0 galaxies is also favored in the dense environments. The models predict a small probability of finding isolated E/S0 galaxies and they should have younger stars on average than their cluster counterparts, as well as assembled their present–day masses by late major mergers (Kauffmann 1996; de Lucia et al. 2006).

A complementary analysis of galaxy morphology and gross photometric properties has been introduced some years ago, namely the *CAS* (concentration, asymmetry and clumpiness) system. This system has been proposed to distinguish galaxies at different stages of evolution (Conselice 2003, and references therein) and it provides the possibility to carry out a physical and quantitative classification based on measurable structural parameters. We present here the measured *CAS* parameters in the *ugriz* bands for the 549 CIG $\cap$ SDSS isolated galaxies.

The outline of the paper is as follows. Section 2 summarizes the relevant past work on CIG morphologies. In §3 the image processing scheme and considerations used to reevaluate morphology for the CIG $\cap$ SDSS galaxies are

presented. In §4 a description of our Atlas of mosaic images for the 549 CIG $\cap$ SDSS galaxies is presented. The results of our classification and morphological analysis, and the calculation of the *CAS* parameters in the *ugriz* bands are presented. Section 5 is a discussion containing a comparison of our morphological classification to previous works (§5.1), a discussion on the bar and ring fractions in spiral galaxies (§5.2), the morphological distortions and formation of isolated E galaxies (§5.3), and the *CAS* parameters in different bands and their correlations with other galaxy properties (§5.4). Finally, in §6 a summary and the main conclusions of this paper are presented.

## 2. CIG MORPHOLOGY IN THE LITERATURE

The morphological classification as well as the environment of each CIG galaxy was originally inspected using the Palomar Observatory Sky Survey (POSS I) images which were based on Kodak blue 103aO and red 103aE emulsions. According to Sulentic (1989), the representative numbers in the CIG were 168 E/S0 and 883 Sa–Sm/Irr. The morphological refinement of the CIG was gradually carried out as new-quality data in the optical and other wavelengths were accumulated since the POSS I era. As the result, for example about one-half of E’s in the original CIG were found to be misclassified (Saucedo–Morales & Biegging 2001). A detailed review on previous works about the morphological refinement for the CIG galaxies is out of the scope of this paper; for a recent review on this see Sulentic et al. (2006; hereafter Sul06). The role of extragalactic databases in collecting and homogenizing data of diverse nature (from photographic, photoelectric and CCD images) has been fundamental. We mention the special role played by NED and HyperLeda databases, which will be used extensively through this work.

The morphological content of the whole CIG sample has been reevaluated by Sul06, who used the digitalized POSS II data. POSS II is based on the IIIaJ and II–IaF emulsions providing higher contrast and resolution than the previous POSS I. Their main results concerning the morphological content are: (1) 82% of the CIG galaxies are spirals (Sa–Sd) with the bulk being luminous systems with small bulges (63% are between Sb and Sc types), and (2) 14% are early-type E/S0 galaxies (the remaining 4% are suspected to be irregular galaxies. Sul06 also reported a considerable number of galaxies in the CIG catalog ( $n = 193$ ) flagged for the presence of nearby companions or signs of distortion likely due to interactions. Those results represent a more uniform and homogeneous reclassification for the whole CIG catalog and provide an excellent frame to test the results of our new morphological reevaluation for 549 CIG galaxies with images available in the SDSS (DR6) database.

Recent examples of detailed morphological reclassifications for CIG galaxies based on optical CCD images, from San Pedro Mártir National Observatory, and extended to the Near-Infrared domain can be found in Hernández-Toledo et al. (2007; 2008).  $H\alpha$  morphological studies in another subsample of CIG isolated spiral galaxies have been reported by Verley et al. (2007).

## 3. THE CIG $\cap$ SDSS DATA SAMPLE AND IMAGE PROCESSING

### 3.1. *Isolated Galaxies from the SDSS DR6. The Data*

The SDSS is a digital photometric and spectroscopic survey obtained with a mosaic camera that images the sky by scanning along great circles at the sidereal rate (Gunn et al. 1998). The imaging data are produced simultaneously in the photometric  $u, g, r, i,$  and  $z$  bands, with effective wavelength bands of 3551, 4770, 6231, 7625, and 9134 Å, respectively (Fukugita et al. 1996) under photometric conditions (Hogg et al. 2001). The SDSS data are reduced by highly automated photometric and spectroscopic reduction pipelines (see Stoughton et al. 2002). Sources are identified, deblended, and photometrically measured (Lupton et al. 2002), and then the magnitudes are calibrated to a standard star network approximately in the AB system (Smith et al. 2002). Very recently the SDSS team made public their DR6 to the astronomical community. SDSS DR6 covers 9583  $deg^2$  of five-band imaging data of the sky and includes spectra, with derived spectroscopic parameters, for 68 770 stars, 790 860 galaxies, and 103 647 quasars. Based on NED and HyperLeda coordinates for the whole CIG sample, all the available SDSS  $ugriz$  band images (scale 0.396 "/pixel) were retrieved from the SDSS archive for a total of 549 entries from CIG (the CIG $\cap$ SDSS sample).

To process the images from the SDSS (DR6) a procedure that i) efficiently detects stars, ii) finds their positions, iii) estimates the nearby sky background and iv) replace the stars in the images by a close representative background, was implemented. For this purpose several routines from the IDL Daophot package were used. To improve the performance of these routines, the signal to noise ratio in the images was enhanced by suppressing high spatial frequency image noise. This task was accomplished by using a small digital low-pass filter (Mighell 1999). After identifying the position of a target galaxy, a next stage starts by creating a mask of about two times the corresponding Petrosian radius above each galaxy. The covering area around a target galaxy was set to protect and preserve the local characteristics of each galaxy image while cleaning the rest of the image of field stars. At the same time, the image sections containing detected stars were substituted by local background values. Mean background is reestimated and subtracted from the whole new image and optionally from a section of the image, depending on the position of the target galaxy within the original CCD frame. The procedure was completely programmed within the IDL platform by using the routines provided by the IDL Astronomy User's Library which includes Daophot. Through this procedure we were able to process thousands of images and repeat the image procedure to find, after trial/error tests, the optimal parameters related to the star subtraction process.

In the next stage, all the images were automatically filtered through a mean Gaussian kernel and at the same time, the diffuse background was canceled out following filter-enhancing techniques (Sofue 1993). A three-component mosaic containing (1) a clean/sky subtracted and logarithmic scaled  $g$ -band image, (2) the corresponding filtered-enhanced version of (1) and (3) the corresponding RGB image, available in the SDSS database were used for each individual galaxy. As a first step of the morphological classification we sorted the sample into E/S0/Sa and Sab-Sm/Irr candidates. Next, differ-

ent kernel values were used to filter and enhance different morphological details in early and late-type galaxies to further proceed with a second classification stage. The resultant images were used to create 1) three-component image mosaics for Sb-Irr galaxies and 2) three-component images plus the corresponding surface brightness and geometric profiles after an isophotal analysis for E/S0/Sa galaxies.

### 3.2. *Morphological Considerations*

Galaxy classification is strongly dependent on the quality of the data employed (s/n ratio and resolution) and of course, on the wavelength. We state here our general criteria to carry out such a classification in the  $g$  band. We expect to find more detailed and reliable structure because of the improved scale and dynamic range of the SDSS database. In order to discuss the optical morphology and its relationship to the global photometric properties, we present the 549 CIG $\cap$ SDSS mosaics, each one including 1) a gray scale  $g$ -band image displayed in logarithmic scale to look for internal/external details; 2) an  $g$  band filtered-enhanced image to look for internal structure in the form of star forming regions, bars, rings and/or structure embedded into dusty regions; for E's this method is useful to reveal fine structure (e.g. dust, shells, broad tides, etc.) underneath the dominant light of the galaxy; and 3) an RGB color image from the SDSS database to visualize the spatial distribution of the SF and other components like dust (blue colors for recent SF and red colors for older populations/dusty components) to complement the structural and morphological analysis.

In the case of E/S0/Sa candidates, besides including the processed images, we use the ISOPHOTE package in IRAF to fit ellipses to the galaxy distribution of light. This package uses an iterative method that starts at a small radius and increases to large radii in a geometrical progression. The galaxy center, position angle and ellipticity were allowed to vary. These isophotal shape parameters help define the morphology of the galaxy. For example, the fourth-order cosine term of the Fourier series is a useful parameter to express the deviation from a perfect ellipse due to the presence of additional light. An excess of light along the major and/or minor axes (disky) is indicated by positive values, while negative values indicate excess light at 45° with respect to these axes (boxy). Each mosaic includes a surface brightness profile and the corresponding geometric profiles of ellipticity ( $\epsilon$ ), Position Angle ( $PA$ ) and  $A_4/B_4$  coefficients of the Fourier series expansions estimated from the  $r$  band images.

#### 3.2.1. *Sab-Sm/Irr Types*

The classification of the sample follows the basic Hubble sequence. For S types we considered the bulge to disk ratio as judged from the observed prominence of the bulge, tightness of the arms, and the degree of resolution of structure along the arms/outer disk. In the majority of the CIG spirals these features are well recognized, however in some cases the presence of structures like dust lanes, prominent knots and the apparent tightening of the arms in the central regions may confuse the identification of inner rings or bars. Outer rings/pseudo-rings (Buta 1995) were also identified when possible. While the presence/absence of a bar was confirmed in some

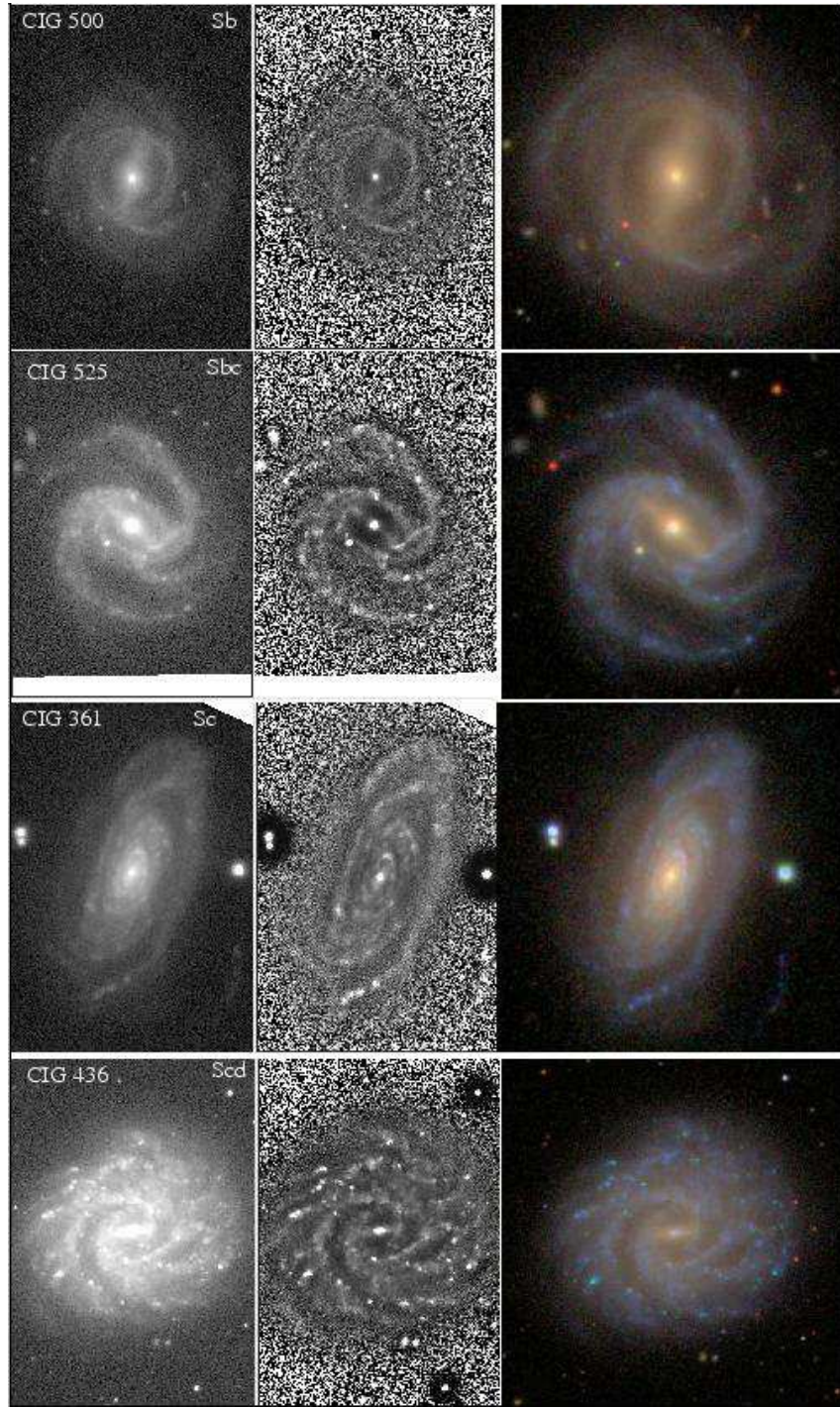


FIG. 1.— CIG 500: a spiral galaxy with a prominent bulge classified as SBb(r). CIG 525: the bulge is less prominent and the arms become to show more definite structure. Classified as SBbc(r). CIG 361: the bulge is even less prominent and the arms show significant fragmentation. Classified as SABc. CIG 436: a late-type spiral with clear fragmentation/resolved structures in the arms. Classified as SBcd(r).

cases (B), in the suspected cases we adopted the (AB) nomenclature convention. In most of the cases when the inclination of the galaxy is greater than  $80^\circ$  (see Table 1) we tend to adopt the classification from the literature.

Figure 1 illustrates our image procedures and shows 4 S galaxies (CIG 500, CIG 525, CIG 361 and CIG 436) that were classified according to the stated criteria. Notice how the bulge is relatively decreasing in importance and the arms become significantly fragmented/resolved

into clumps indicating, from top to bottom, Sb, Sbc, Sc, and Scd types. Some main structural features like bars and rings were identified and sometimes suspected. Each galaxy is identified by its CIG number and the corresponding morphological type.

The first row of Figure 1 shows CIG 500 displayed in logarithmic scale (left-panel). The prominence of the bulge/bar region and at the same time the smoothness of a not so tightly wound set of arms are appreci-

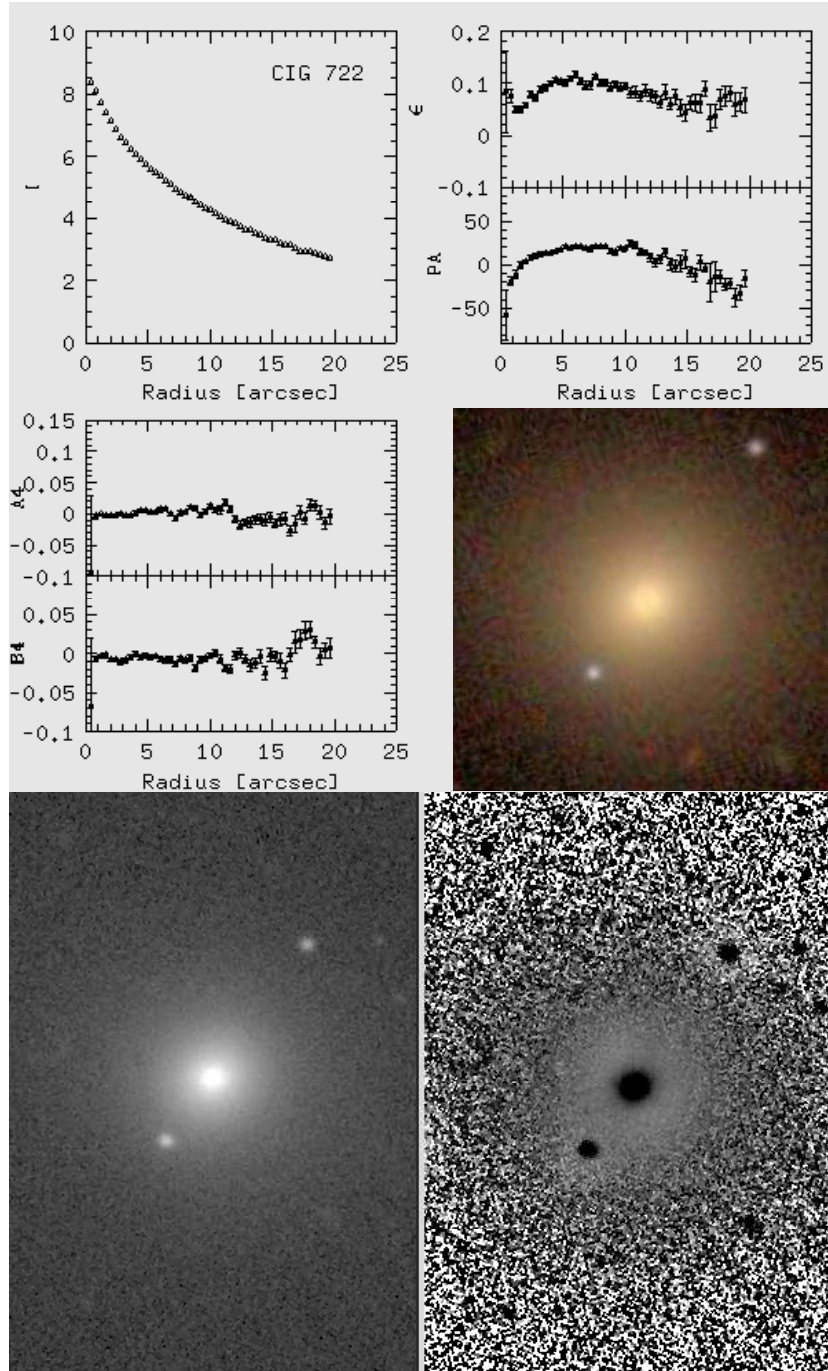


FIG. 2.— CIG 722: a prototype of an elliptical galaxy. The upper panels show the Surface brightness, the ellipticity  $\epsilon$ , Position Angle  $PA$  radial profiles and  $A_4/B_4$  coefficients of the Fourier series expansions of deviations of a pure ellipse in the  $g$ -band. The lower panels show the RGB color map form SDSS, the logarithmic-scaled  $g$ -band image and its filtered-enhanced version.

ated. The  $g$ -band filtered-enhanced image (middle panel) let us appreciate more detailed structure along the bar, ring, and arms. The filtered-enhancing techniques (Sofue 1993) allow the subtraction of the diffuse background in a convenient way to discuss different morphological details. The RGB composed image (right panel) from the SDSS database complement and reinforces our view of a prominent bulge/bar region and the smoothness of the arms. While HyperLeda classifies this galaxy as *Sab* NED reports an  $(R')SAB(r)ab$  type with an outer pseudo-ring

and an internal ring. The most recent reevaluation by Sul06 classifies CIG 500 as SBb. We classify this galaxy as SBb( $r$ ).

The second row in Figure 1 shows CIG 525. The logarithmic image shows a slightly less prominent bulge but a significant bar and moderately opened arms. The  $g$ -band filtered-enhanced image shows more detailed structure along the arms and the inner ring. The RGB image complements our view emphasizing detailed structure along the arms. While HyperLeda, NED and Sul06 classify this

galaxy as Sb, we classify CIG 525 as SBbc(*r*).

The third row of Figure 1 shows CIG 361. The logarithmic image shows a galaxy with a less prominent bulge but with a set of quite opened arms showing significant fragmentation. The filtered-enhancing image let us suspect about a central barred region and emphasizes the fragmentation along the arms. The RGB SDSS image clearly supports a detailed view of all these features. While HyperLeda and NED classify this galaxy as Sb, Sul06 classifies CIG 361 as Sab. In contrast, and from the observed structure, we classify CIG 361 as SABc.

Finally the fourth row in Figure 1 shows CIG 436. The bulge appears not so significant and the arms are strongly fragmented/resolved into clumps. An inner ring and a bar region are readily appreciated. While HyperLeda classifies this galaxy as SBc, NED, Sul06 and we classify CIG 436 as SBcd. A more detailed classification from our images is SBcd(*r*).

### 3.2.2. *E/S0 Types*

For early-type (E/S0/Sa) candidates, besides a careful inspection to the processed images, we carried out an evaluation of the geometrical parameters after an isophotal analysis. The ellipticity  $\epsilon$ , position angle  $PA$ , coefficients of the Fourier series expansions  $A_4$ ,  $B_4$  and the surface brightness radial profile are also presented for each galaxy. Although the absolute value of the  $A_4$  parameter depends on the inclination of the galaxy to the line of sight, its sign is useful to detect subtle disk features in the early-type candidates. The presence of disk isophotes is one criterion for assigning a galaxy to the lenticular class. However, disks or disk components have also been found among the E class (e.g., Bender 1988; Nieto et al. 1988). A galaxy was judged to be E if the  $A_4$  parameter showed: 1) no significant boxy ( $A_4 < 0$ ) or disk ( $A_4 > 0$ ) trend in the outer parts, or 2) a generally boxy ( $A_4 < 0$ ) character in the outer parts and if in addition, the surface brightness profile showed 3) the absence of a linear component in the surface brightness profile. Central diskiness is considered not enough for an S0 classification. Additionally we paid attention to changes in the  $\epsilon$  and  $PA$  radial profiles.

For an E type we should not observe a significant change in both  $\epsilon$  and  $PA$ , while in the case of an S0, more significant changes in these parameters could be showing evidence of a disks. The presence of structure in the outer regions of E's like rings/shells and diffuse haloes (DH) could mimic an external disk as viewed from the point of view of the geometric profiles. However, if our additional image processing did not show evidence of definite features, we kept the galaxy type as E. The surface brightness radial profile is also an important tool to discriminate between E/S0 types. It is known that in the E's the surface brightness profile follows either a de Vaucouleurs or a more general Sérsic law. When the profile presents a significant deflection in the curvature into a linear regime (not associated to other internal structures like inner disks, rings or bars), this could be evidencing the presence of an external disk. Figures 2 and 3 illustrate our imaging procedures for identifying E and S0 galaxies. Each galaxy is identified by its CIG number.

Figure 2 shows CIG 722 as a prototype of an E galaxy. The upper panels show the  $g$ -band surface brightness,  $\epsilon$ ,  $PA$  radial profiles and  $A_4/B_4$  coefficients of the Fourier

series expansions of deviations from pure ellipses. While the surface brightness profile shows no trace of a linear component in the outer regions, the  $A_4$  and  $B_4$  coefficients of the Fourier series expansions do not show any significant tendency towards diskiness or boxiness and at the same time, the  $\epsilon$  and  $PA$  radial profiles show a non-significant trend from the inner to the outer regions. The lower panels show an RGB color map from the SDSS database, a logarithmic-scaled  $g$ -band image and its corresponding filtered-enhanced version. A uniform color along the face of this galaxy is appreciated. The  $g$ -band filtered-enhanced image shows in addition, some sort of faint external DH's. We caution the reader about the existence of these DH's in some of our E/S0 candidates and that care must be taken about its interpretation.

Similarly as Figure 2, Figure 3 shows CIG 16 as a prototype of a S0 galaxy. The surface brightness profile clearly shows an inflection most probably caused by the underlying disk structure (caution must be paid for the presence of inner rings or bars), the  $A_4$  and  $B_4$  coefficients of the Fourier series expansions show the tendency to deviate towards disk shapes but this is more clear at the outskirts. At the same time,  $\epsilon$  indicates a clear change from the inner to the outer regions reaching a maximum and then a more definite value at the outer disk region while  $PA$  basically indicates the orientation of the semi-major axis. The lower panels present the RGB color map from the SDSS database, the logarithmic-scaled  $g$ -band image, and its filtered-enhanced version. This time, a faint elongated component along the main  $PA$  of the galaxy can be appreciated in the geometric profiles. The  $g$ -band filtered-enhanced image let us visualize that disk structure suggested in the geometric profiles.

### 3.2.3. *S0/Sa Types*

Another relevant goal in our study is to isolate as much as possible subtle differences between lenticular S0 and Sa spirals. The advantages offered by the SDSS images allow for a systematic search of fainter features that could point to a more definite morphological classification. We observed the combined behavior of both  $\epsilon$  and  $PA$  radial profiles as an auxiliary tool to disentangle among S0/Sa cases. Significant but not necessarily coupled changes in  $\epsilon$  and  $PA$  radial profiles should be evidencing the presence of additional structure (in an already identified disk) in the form of arms, outer rings or envelopes. If further additional image processing did not show definite evidence of those features, we kept the galaxy type as lenticular. On the contrary, if the evidence about features like faint arms are definite, we classify the galaxy as Sa.

Figure 4 illustrates CIG 393 as a prototype of a very early-type Sa galaxy. While originally suspected as a peculiar S0 candidate from its appearance in both the  $g$ -band and RGB SDSS images, the  $A_4$  and  $B_4$  coefficients of the Fourier series expansions suggest the presence of a disk from the inner to the outskirts and at the same time,  $\epsilon$  and  $PA$  show a clear non-coupled change resembling additional structure(s), likely a set of smooth wide and tightly-wounded arms. The color component in the central regions appreciated from the RGB image also suggests the presence of an extra component. This time the  $g$ -band filtered-enhanced image allows to see

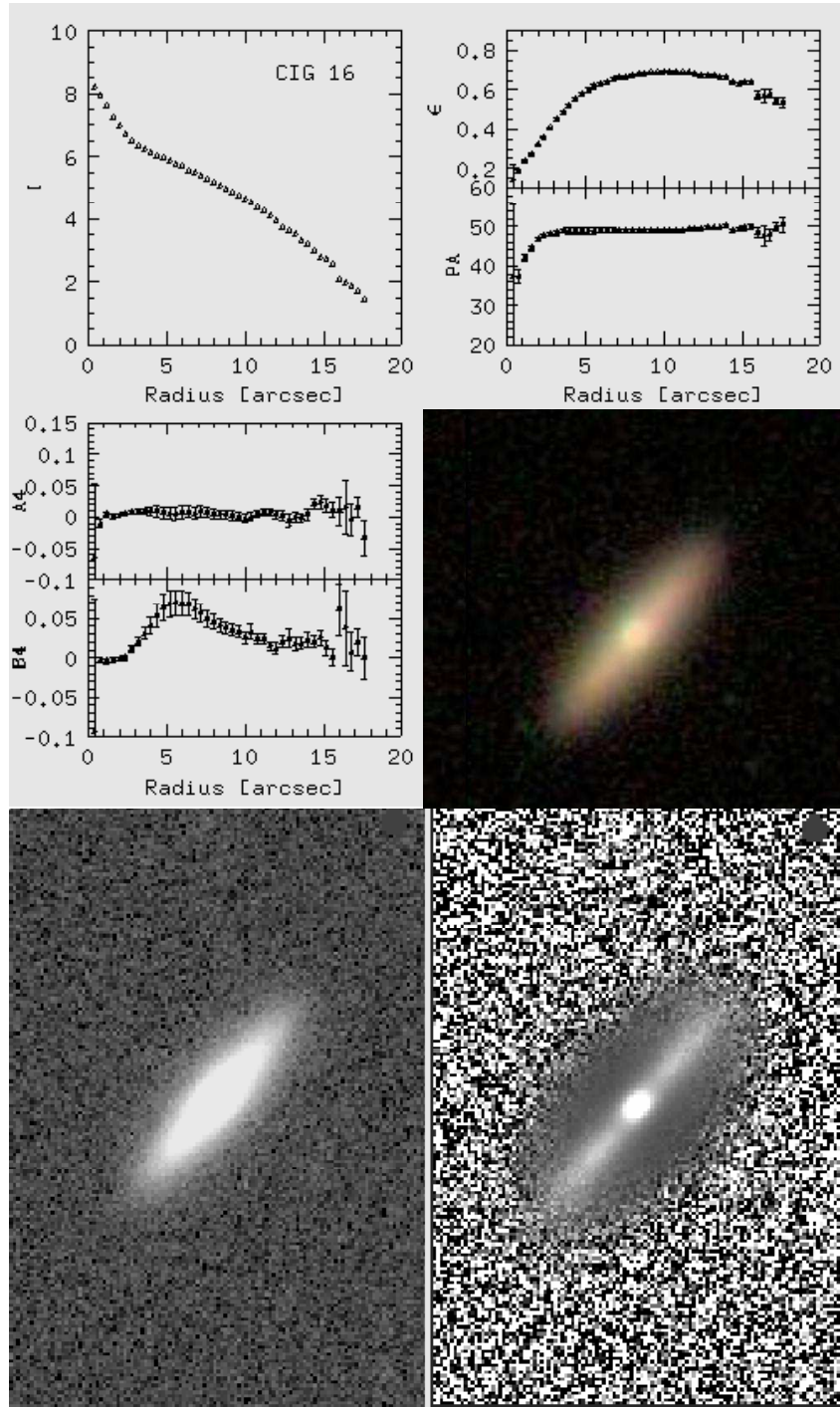


FIG. 3.— CIG 16: a prototype of a lenticular galaxy. Same as in Figure 2.

that additional component in the form of two inner arms that become wide, smooth but still tight at the outskirts. The oval shape of the bulge region suggest a bar signature that  $\epsilon$  and  $PA$  marginally detect. (c.f. Wozniak et al. 1995). Cases like CIG 393 clearly illustrates the advantages of the higher resolution and depth of the SDSS survey.

### 3.3. Physical Morphology

Physical morphology has appeared as an alternative for classifying galaxies on the basis of measurable structural properties rather than on a visual classification (see Morgan & Osterbrock 1969; Abraham et al. 1996; Conselice 1997; Bershad, Jangren & Conselice 2000, among others). Conselice (2003, and more references therein) has provided a useful framework for classifying galaxies closely tied to underlying physical processes and properties. Conselice (2003; hereafter C2003) argues that the major ongoing and past formation modes of galaxies can

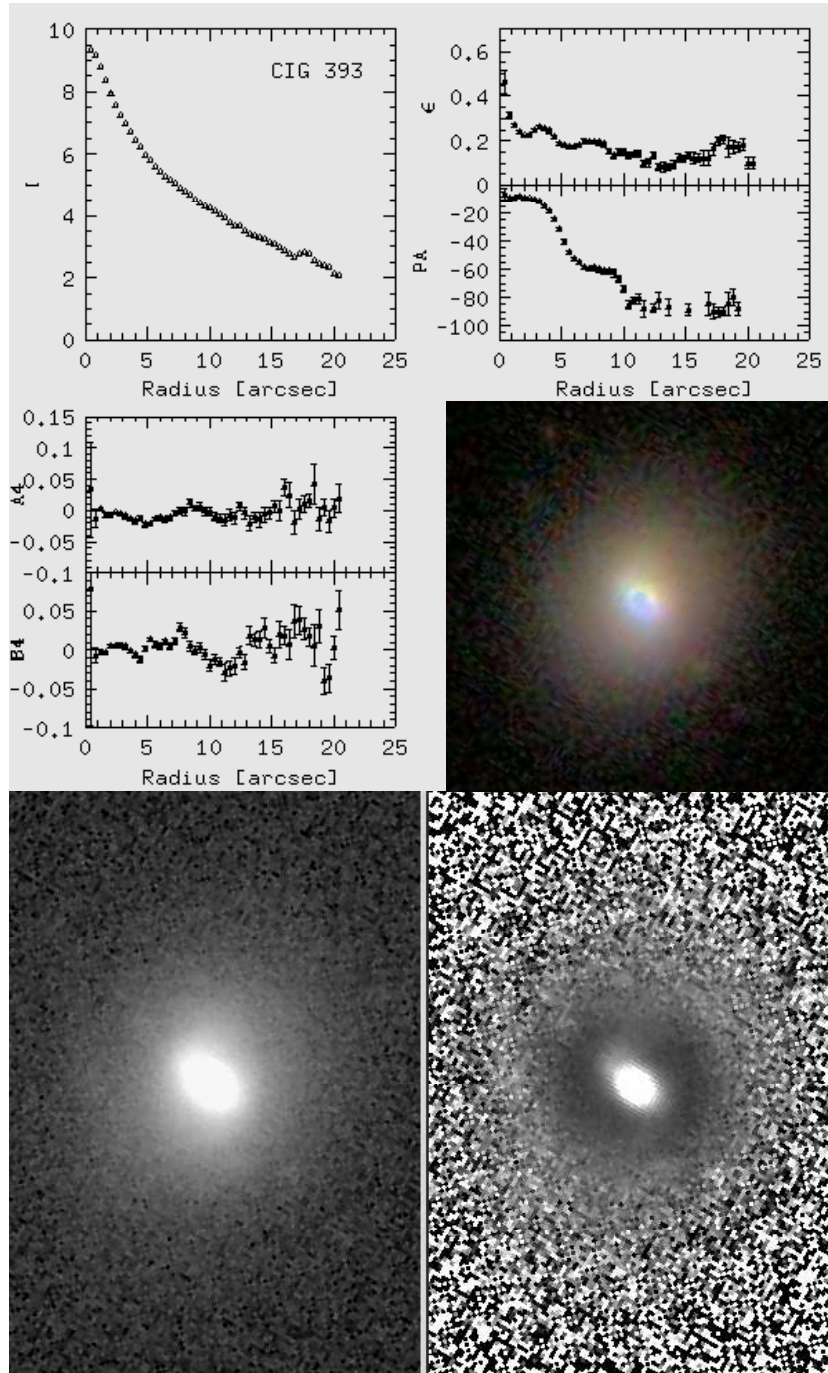


FIG. 4.— CIG 393: a prototype of a very early-type spiral galaxy. Same as in Figure 2.

be distinguished using three model-independent structural (photometric) parameters, which allow for a robust classification system. These parameters are the concentration of stellar light ( $C$ ), its asymmetric distribution ( $A$ ), and a measure of its clumpiness ( $S$ ).

We present our estimate of the  $CAS$  parameters in the  $r$  band and discuss some trends of the  $CAS$  parameters at the SDSS  $ugriz$  passbands for the retrieved sample of CIG galaxies. The  $CAS$  characterization of this CIG galaxies is also helpful as a comparative sample for interpreting similar results of other surveys that sample

galaxies in similar (Hernández-Toledo et al. 2007; 2008) or wide range of environments (e.g., C2003; Hernández-Toledo et al. 2005; 2006).

We briefly review each one of the  $CAS$  parameters.

*Concentration of light  $C$ .*— The concentration index  $C$  is defined as the ratio of the 80% to 20% curve of growth radii ( $r_{80}$ ,  $r_{20}$ ), within 1.5 times the Petrosian inverted radius at  $r(\eta = 0.2)$  ( $r'_p$ ) normalized by a logarithm:  $C = 5 \times \log(r_{80\%}/r_{20\%})$  (see for more details C2003). The concentration is related to the galaxy light (or stellar mass) distributions.

*Asymmetry A.*- The asymmetry index is the number computed when a galaxy is rotated  $180^\circ$  from its center and then subtracted from its pre-rotated image, and the summation of the intensities of the absolute value residuals of this subtraction are compared with the original galaxy flux (see for more details C2003). This parameter is also measured within  $1.5 \times r'_P$ . The  $A$  index is sensitive to any feature that produces asymmetric light distributions. This includes galaxy interactions/mergers, large star-forming regions, and projection effects such as dust lanes (Conselice 1997; Conselice et al. 2000).

*Clumpiness S.*- Galaxies undergoing SF are very patchy and contain large amounts of light at high spatial frequency. To quantify this, the clumpiness index  $S$  is defined as the ratio of the amount of light contained in high frequency structures to the total amount of light in the galaxy within  $1.5 \times r'_P$  (C2003). The  $S$  parameter, because of its morphological nature, is sensitive to dust lanes and inclination (C2003).

*Measurement of CAS parameters.*- The measurement of the  $CAS$  parameters for the CIG galaxies was carried out in several steps: (i) close field stars were removed from each image; (ii) sky background was removed from the images; (iii) the center of each galaxy was considered as the barycenter of the light distribution and the starting point for measurements.

The  $CAS$  parameters for all the S isolated galaxies were estimated directly, i.e. CIG galaxies are not influenced by light contamination from any other galaxy of similar size in the neighborhood (isolation criteria). Galaxies with high inclinations or axis ratios could introduce systematic biased trends in the values of the  $CAS$  parameters (C2003). CIG galaxies whose apparent axial ratios yield “inclinations” larger than  $80^\circ$  are represented as open circles on the corresponding plots.

To obtain good  $CAS$  estimates, the images need to be carefully revised for the possible existence of the following problems (that should be eliminated as much as possible): (i) images with poor quality or low s/n ratio; (ii) overlapping bright stars within galaxies; (iii) galaxies placed at the border of the CCD detector; (iv) very bright diffraction spikes from nearby stars crossing a galaxy; (v) galaxies embedded in diffuse light of other sources; (vi) clear cases of merger candidates.

In the present paper, all those factors have not necessarily been eliminated. Instead a more statistical approach have been assumed by restricting the analysis to more definite ranges of  $CAS$  values in each band such that values outside those intervals (most likely CIG galaxies which images suffer from one or more of the above mentioned drawbacks) were eliminated from the  $CAS$  analysis, leaving us with a different final number of galaxies in each band. In the  $r$  band this number amounts to 390 galaxies.

## 4. RESULTS

### 4.1. The Atlas

Each of the 549 isolated  $CIG \cap SDSS$  galaxies are presented in the form of a mosaic. For S galaxies of types later than Sa, we include, from upper-left to lower-right panel: (1) a gray scale  $g$ -band image displayed in logarithmic scale, (2) an  $g$  band filtered-enhanced version of the image in 1), and (3) an RGB color image from the

TABLE 1  
RESULTS OF THE NEW MORPHOLOGICAL  
CLASSIFICATION FOR THE  $CIG \cap SDSS$  SAMPLE  
BASED ON THE AVAILABLE SDSS (DR6) DATA.

Type	$n$	$n/1018$	$n_{SDSS}$	$n_{SDSS}/539$
E	58	0.057	19	0.035
E/S0	14	0.014	-	-
S0	67	0.066	27	0.050
S0/a	19	0.019	-	-
Sa	13	0.013	35	0.065
Sab	52	0.051	42	0.078
Sb	159	0.156	69	0.128
Sbc	200	0.196	91	0.169
Sc	278	0.273	161	0.299
Scd	61	0.060	44	0.082
Sd	41	0.040	28	0.052
Sdm	15	0.015	7	0.013
Sm	15	0.015	9	0.017
Im	26	0.026	5	0.009
E-S0	125	0.122	46	0.085
Sa-Sd	804	0.790	470	0.872
Sb-Sc	637	0.626	321	0.596

SDSS database (See Figure 1).

For E/S0/Sa galaxies, besides including the processed images 1), 2) and 3) above, additional surface brightness profiles and geometric profiles (ellipticity  $\epsilon$ , Position Angle  $PA$  and  $A_4/B_4$  coefficients of the Fourier series expansions of deviations of a pure ellipse) from the  $r$  band images are provided (See Figures 2, 3 and 4).

All the 549 mosaic images in the present reevaluation can be reviewed on the web-site (<http://132.248.1.210>).

### 4.2. Optical Morphology

Table 1 reports our morphological reevaluation of 539 CIG galaxies after eliminating 10 galaxies in common to the lists of possible interacting galaxies by Sul06. Columns (1), (2) and (3) give the morphological type, the number  $n$  of galaxies in each morphological type and the corresponding fraction  $n/1018$  as reported in Table 2 of Sul06. Similarly, Columns (4) and (5) give the number  $n_{SDSS}$  of retrieved galaxies in this work and the estimated fraction  $n_{SDSS}/539$  for each morphological type according to our reevaluation.

Figure 5 shows the differential and cumulative histograms of the results in Table 1. Solid lines correspond to the reevaluated fractions in this work. We find that the median type of the  $CIG \cap SDSS$  sample is Sbc, with 35% of the galaxies being earlier than Sbc, and 65% being Sbc type or latter. A fraction of 90.20% are S galaxies in the range of Sa–Sm types and only 8.53% are of early-type (E–S0); the remaining 1.27% are irregulars (0.9%) and unclassifiable galaxies (0.37%, which corresponds to two objects). The fraction of early-type spirals (Sa and Sab) amounts to about 14%. These results are at odds with those by Sul06 (dashed line in Fig. 5), who classified 14% of the CIG galaxies as E/S0 types and 82% as Sa-Sd types. Among the spirals, only 6% were classified as early-type Sa–Sab spirals. Notice that we attempted for a cleaner classification avoiding transition E/S0 and S0/Sa cases. A suitable processing of the SDSS images complemented with color information permit a better spatial discrimination of morphological details in spiral galaxies like the prominence and extent of

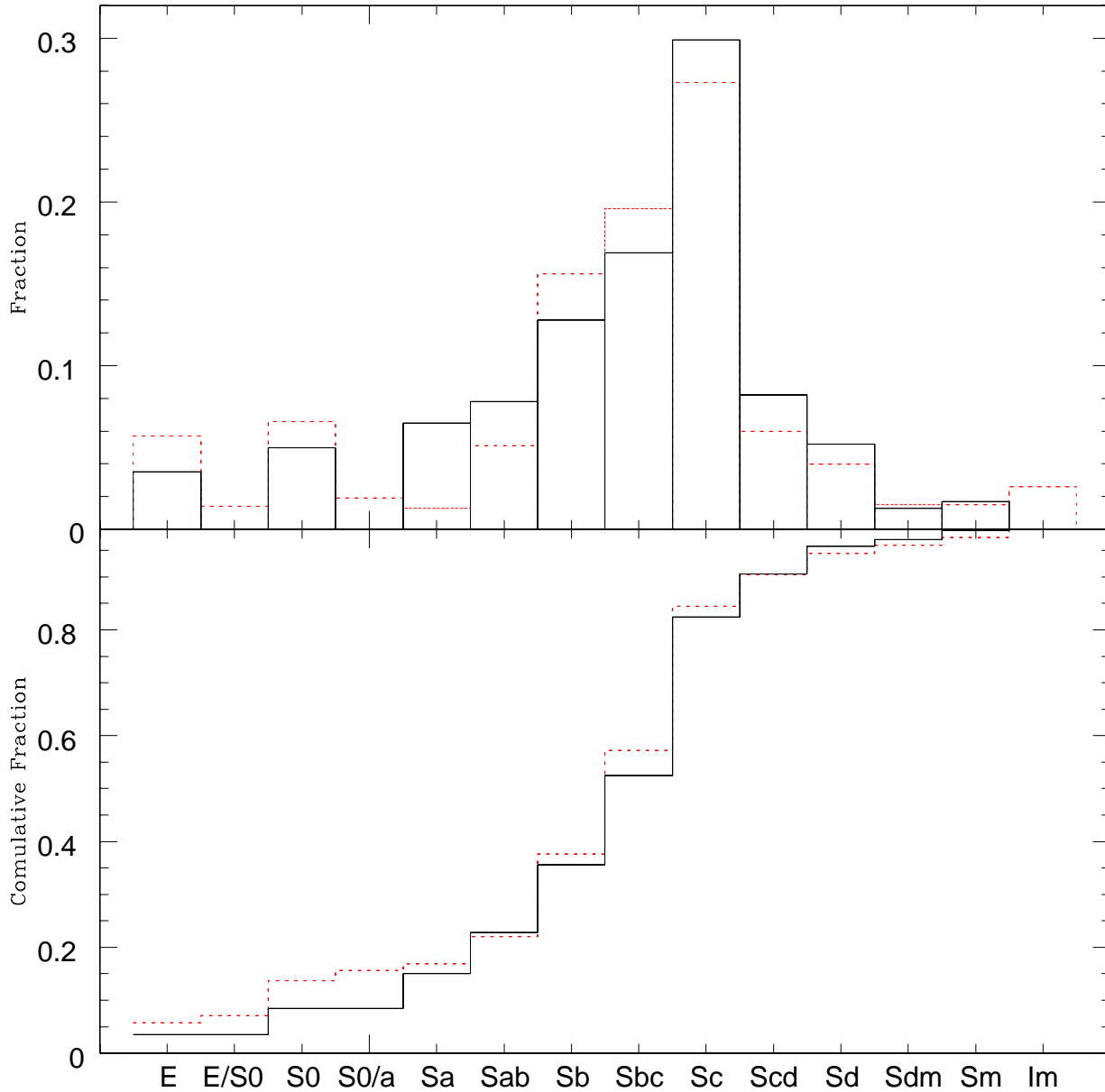


FIG. 5.— Upper panel: Normalized histogram of morphological types for the 539 CIG galaxies analyzed with our image procedures by using the SDSS (DR6) database (solid line). For comparison, the results from Sul06 for a sample of 1018 CIG galaxies classified from the POSS II images is also plotted (dashed line). Lower panel: Cumulative Fraction of morphological types found in this work (solid line) and in Sul06 (dashed line).

bulges. Higher resolution is important to distinguish between inner rings and ring-like features produced by the tightening of the arms, the fragmentation degree of the arms or structures like bars, clumps, dust lanes, among others. Our filtering process enhances high spatial frequency structures in S's and (depending on the kernel size) in E's too.

Our preliminary bar identification is based on a careful visual inspection of the  $r$ -band clean/subtracted images as well as the corresponding filtered-enhanced and RGB images. For early-type galaxies, the surface brightness

and geometric profiles, after an isophotal analysis, were also used to define the presence of a bar. As the result, we identified 292 disk galaxies with bars, which accounts for 59.2% of the disk galaxies in the  $\text{CIG} \cap \text{SDSS}$  sample (25.5% with clear bars, SB type, and 33.7% with weak or suspected bars, SAB type). Because bar detection becomes difficult in highly inclined galaxies, we adopted also the standard procedure of excluding objects with an inclination  $i \geq 60^\circ$  ( $\approx 56\%$  of the disk galaxy subsample). For the  $i \leq 60^\circ$  sub-sample, we find a fraction of barred galaxies of 65.8% (SA=35% and SAB=30.8%).

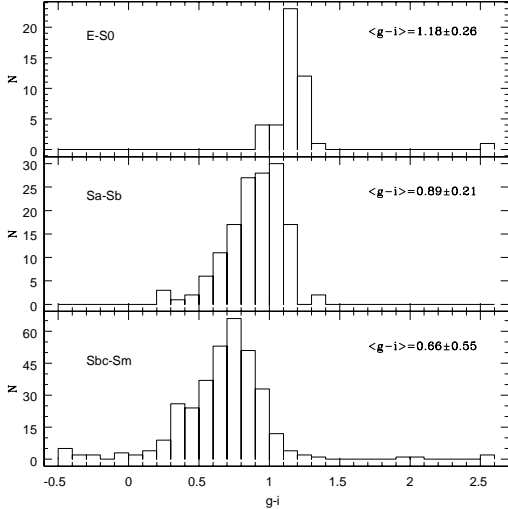


FIG. 6.—  $(g-i)$  color histograms for the CIG galaxies sorted into E/S0 types (upper panel), SaSb types (middle panel), and SbcSm galaxies (lower panel).

The bar fraction in early type spirals (Sa–Sb) is 65% and is almost the same one (66%) in late types (Sbc–Sm/Irr), though we caution the reader about possible biases in this result (see §§5.2 for a discussion). A more careful analysis including more appropriate ways to detect bars for this sample will be presented elsewhere. Similarly, the information for rings in disk galaxies (inner, outer rings and pseudo-rings) in our sample is tentatively available for 164 galaxies accounting to 33.3% of the disk galaxies.

Table 2 shows a comparison of our morphological results against the corresponding information from the literature. Only CIG galaxies with  $V_{rad} > 1000 \text{ km s}^{-1}$  are included. Column (1) is the CIG cataloged number, Column (2) the Hubble Type from Lyon Extragalactic Database (HyperLeda), Column (3) the Hubble Type from NED, Column (4) the Hubble Type from Sul06 Column (5) the Hubble Type from this work, and finally Column (6) the inclination to the line-of-sight as reported in the HyperLeda database.

Table 3 shows similar results as Table 2 but for CIG galaxies with ( $V_r < 1000 \text{ km s}^{-1}$ ). Although at  $V_r < 1000 \text{ km s}^{-1}$  the morphology is more difficult to evaluate in terms of isolation, we have proceeded because in nearby galaxies more detailed structural information is generally available, thus providing another test on the reliability of our classification. The inclination is included as a guide to evaluate the reliability of the classification.

#### 4.3. CAS Results

The CAS parameters in the recent literature are frequently reported in the Johnson-Cousins  $R$  band. Given the similarity in definition (both in  $\lambda_c$  and  $\Delta\lambda$ ) between  $R$  and the SDSS  $r$  band photometric systems, a similarity in the estimated CAS values is expected. Thus we report here the CAS parameters and the corresponding errors in the  $r$  band for a sample of 390 CIG galaxies. The CAS parameters are listed in Table 4. The CAS values for the CIG galaxies in other bands can be provided by the authors upon request.

We have sorted the CIG sample into three groups: early- and late-type spirals (SaSb and SbcSm, respec-

TABLE 2  
DETAILED MORPHOLOGY FOR THE CIG $\cap$ SDSS SAMPLE ( $V_r > 1000 \text{ km s}^{-1}$ ).

CIG	Leda	NED	Sulentic 2006	This work	incl
CIG 0011	SABc	SAB(s)c?	Sbc	SABc	67.48
CIG 0012	Sbc	Sb	Sb	Sbc	79.45
CIG 0016	Sbc	S0	S0	S0	64.22
CIG 0019	S0-a	S0	S0	SABa	90.00
CIG 0033	SABc	SAB(rs)cd	Sb	SABc	53.76
CIG 0056	Sb	SB(rs)b	Sb	RSBb(r)	52.52
CIG 0060	Sb	Sb	Sd	SABc	62.87
CIG 0081	Sb	Sb	S0	S0	84.80
CIG 0187	SABb	SAB(s)bc	Sc	SBbc	23.76
CIG 0189	E	Sa	E	E	90.00
:					

TABLE 3  
DETAILED MORPHOLOGY FOR THE CIG $\cap$ SDSS SAMPLE  
( $V_r < 1000 \text{ km s}^{-1}$ ).

CIG	Leda	NED	This work	incl
CIG 0190	IB	Im	Irr	62.62
CIG 0193	Scd	SA(s)d	SABcd	61.27
CIG 0224	Scd	SB(rs)d	SBd	20.61
CIG 0235	SBd	SB(s)mpec	Sd	68.71
CIG 0265	Sbc	SABdm	SABdm	62.44
CIG 0324	Sb	SA(r)b	SABa	68
CIG 0347	SABb	SB(s)d	SBc	56
CIG 0388	IB	Im	Irr	59.88
CIG 0428	SBc	SB(rs)cd	SBcd	62.69
CIG 0434	I	Im	Sm	24.59
:				

tively) and E/S0 galaxies. The corresponding average and standard deviation values of the CAS parameters are listed in Table 5.

In spite of the different zero-point scales that define the SDSS  $r$  band and the Johnson-Cousins  $R$  band systems, we find similar values as those reported in the  $R$  band by Conselice (2003) for the Frei et al. (1996) sample of non-interacting galaxies and also for smaller subsamples of CIG galaxies in Hernández-Toledo et al. (2007; 2008).

#### 4.4. General properties

We have calculated the absolute magnitudes in  $g$ ,  $r$ , and  $i$  bands for our sample of 539 CIG $\cap$ SDSS galaxies by using the HyperLeda distance modulus with  $H_0 = 70 \text{ km s}^{-1} \text{ Mpc}^{-1}$ . We have used the apparent magnitudes corrected by Galaxy extinction ( $A_\lambda^g[\text{mag}]$ ) given for each galaxy in the SDSS database; the corrections are based on the Schlegel et al. (1998) Galaxy maps. For the 493 disk galaxies in our sample, we have further corrected the magnitudes by internal extinction. Several pieces of evidence suggest that the fraction of dust is larger for bigger galaxies. Therefore, the internal extinction correction should depend not only on inclination but also on galaxy scale:  $A_\lambda^i[\text{mag}] = \gamma_\lambda \log(a/b)$ , where  $a/b$  is the major-to-minor axis ratio (taken from HyperLeda), and  $\gamma_\lambda$  is a scale-dependent coefficient in the given passband  $\lambda$ . From an empirical analysis, Tully et al. (1998) inferred the coefficients  $\gamma_\lambda$  in the  $BRIC$  bands as a function of the galaxy maximum circular velocity. From their data (reported explicitly in Tully & Pierce

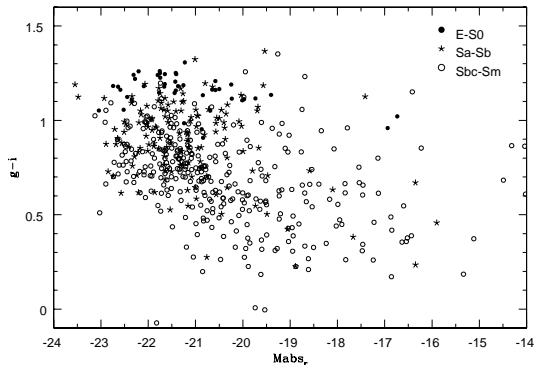


FIG. 7.— Color-Magnitude ( $g-i$  vs  $M_r$ ) diagram for the CIG galaxies sorted into E/S0 types (solid circles), SaSb types (asterisks), and SbcSm galaxies (open circles).

TABLE 4  
CAS STRUCTURAL PARAMETERS AND THEIR ERRORS IN THE  $r$  BAND FOR THE CIG $\cap$ SDSS SAMPLE.

CIG	C	errC	A	errA	S	errS
CIG0011	3.363	0.084	0.176	0.061	0.060	0.013
CIG0012	3.169	0.166	0.302	0.040	0.230	0.020
CIG0016	3.603	0.371	0.095	0.007	0.190	0.008
CIG0019	3.686	0.339	0.103	0.006	0.120	0.005
CIG0033	2.962	0.105	0.190	0.017	0.380	0.018
CIG0056	4.193	0.128	0.174	0.020	-0.030	0.004
CIG0060	2.723	0.189	0.225	0.020	0.320	0.018
CIG0081	4.107	0.249	0.085	0.005	0.020	0.001
CIG0187	3.224	0.072	0.207	0.066	0.600	0.043
CIG0189	4.446	0.174	0.128	0.007	0.280	0.009

2000), Hernández-Toledo et al. (2007) have carried out linear correlations of these calculated coefficients with the corresponding magnitudes *not corrected* for internal extinction,  $M_\lambda^b$ . Here, we interpolate these linear correlations to the SDSS  $gri$  bands and obtain the following approximate coefficients:

$$\begin{aligned} \gamma_g[\text{mag}] &= -6.00 - 0.38M_g^b, \\ \gamma_r[\text{mag}] &= -4.00 - 0.25M_r^b, \\ \gamma_i[\text{mag}] &= -3.60 - 0.21M_i^b. \end{aligned} \quad (1)$$

These coefficients are not valid for low-luminosity galaxies (see Hernández-Toledo et al. 2007 for the lower limits in the  $BVRiK$  bands); for the few cases when  $\gamma_\lambda < 0$ , we set  $\gamma_\lambda = 0$ . We stress that the internal extinction correction suggested here is of statistical nature and it provides only an approximation to a complicated problem, however, it is certainly better than not correcting the data at all for internal extinction. The final corrected magnitude for disk galaxies is then  $M_\lambda^{b,i} = M_\lambda - A_\lambda^b - A_\lambda^i$ .

By using the corrected absolute magnitudes, we are able to calculate the galaxy corrected colors. In Fig. 6 the  $g-i$  color histograms of the 539 CIG $\cap$ SDSS galaxies separated into three morphological ranges are plotted. The averages and  $1\sigma$  dispersions of  $g-i$  for the E/S0,

TABLE 5  
MEAN  $r$  BAND CAS PARAMETERS AND THE CORRESPONDING  $1\sigma$  FOR CIG $\cap$ SDSS GALAXIES ACCORDING TO MORPHOLOGICAL TYPES.

CAS	E/S0	SaSb	SbcSm
C	$3.81 \pm 0.46$	$3.58 \pm 0.52$	$2.97 \pm 0.49$
A	$0.09 \pm 0.03$	$0.14 \pm 0.06$	$0.20 \pm 0.07$
S	$0.08 \pm 0.10$	$0.16 \pm 0.16$	$0.25 \pm 0.18$

Sa-Sb, and Sbc-Sm/Irr morphology ranges are  $1.18 \pm 0.26$ ,  $0.89 \pm 0.21$ , and  $0.66 \pm 0.55$ , respectively. Notice that in the case of E/S0 galaxies no internal extinction correction was applied.

Figure 7 shows the color-magnitude diagram for all the sample, again separated into three morphological ranges (plotted with different symbols). The E/S0 galaxies occupy a quite flat and narrow region in the diagram, while for disk galaxies a loose trend of redder colors as their are brighter is seen, but with a large scatter. The average  $r$ -band absolute magnitudes are  $< -20.91 \pm 2.21 >$ ,  $< -21.02 \pm 1.61 >$ , and  $< -19.84 \pm 2.84 >$ , for E/S0, SaSb and galaxies later than Sbc types, respectively. From these results, we remark that (i) in isolated environments, there is a paucity of luminous E/S0 galaxies, and (ii) the average luminosity of E/S0 galaxies is the same as that in early-type spirals and slightly more luminous than late-type spirals. Park et al. (1994) first quantified the paucity of luminous galaxies at very low environments, they studied the distribution of local density around galaxies showing that regions of moderate and high density contain both very bright ( $M \leq M_* = -19.2 + 5 \log h$ ) and fainter galaxies, but that voids preferentially harbor fainter galaxies (approximately  $2\sigma$  significance level). This last result was later confirmed by Hoyle et al. (2005) by studying the luminosity function of void galaxies in the SDSS.

Notice that our results are in contrast to those in Sul06 where late-type spirals were found to be more luminous on average than E/S0 galaxies. Park et al. (2007) examined the color-magnitude ( $u-r$  vs  $M_r$ ) diagram for early and late-type SDSS galaxies located in high and low density environments, finding a very slight dependence of the location of the early-type SDSS galaxies on the density field and a stronger dependence of the late-type colors on environment.

## 5. DISCUSSION

### 5.1. Optical morphology: comparison with previous works

Figure 8 shows a set of histograms comparing the results of our morphological reevaluation against those in the literature. The upper left panel compares our morphological types vs HyperLeda ( $\Delta T = T_{Ours} - T_{Leda}$ ). The upper-right panel compares our morphological types vs NED ( $\Delta T = T_{Ours} - T_{NED}$ ) and finally, the lower-left panel is a comparison of our results vs those from the morphological reevaluation by Sul06 ( $\Delta T = T_{Ours} - T_{Sul06}$ ). The type code number from RC3 and the additional convention suggested for early types in Sul06 were adopted.

Out from 488 galaxies in common with HyperLeda,

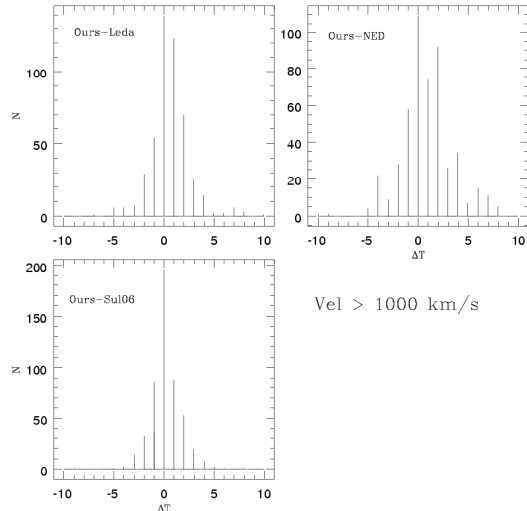


FIG. 8.— Histograms of morphological type differences  $\Delta T = T_{ours} - T_{other}$  for galaxies with  $V > 1000$ , where  $T_{ours}$  is the reevaluated morphological type in this work, and  $T_{other}$  is the morphological type reported in LEDA (upper left panel), NED (upper right panel), and Sul06 (lower panel).

29% have  $\Delta T = 0$  and up to 64% have a difference  $|\Delta T| < 2$ . One third more show larger morphological differences that appear biased towards small positive differences. Similarly, from 496 galaxies in common with NED, 22% have  $\Delta T = 0$  and up to 49% of the sample have  $|\Delta T| < 2$ . This time a larger fraction from the complementary 50% are distributed towards small positive differences. This suggests that in spite of the large dispersion ( $\Delta T = 10$ ) shown in both plots, HyperLeda appears to contain more reliable morphological information previous to the POSS II reevaluation from Sul06. The lower panel of Figure 8 shows that from 502 galaxies in common with Sul06, 40% have  $\Delta T = 0$  and up to 74% of them have  $|\Delta T| < 2$ , indicating a closer agreement in the derived types. The dispersion has significantly decreased ( $\Delta T = 5$ ) and only 25% of the sample is distributed evenly in this range. Only a slight difference is still appreciated first in the negative  $\Delta T = -2$  side and then in the positive  $\Delta T > 2$  side, emphasizing the ability of the SDSS data and the corresponding processing to resolve finer morphological details either in early and late-type galaxies.

Figure 9 shows similar results as those in Figure 8 but for CIG galaxies with  $V_r < 1000 \text{ km s}^{-1}$ . This time the histograms compare of our results against those in HyperLeda (upper left panel), NED (upper-right panel) and other authors as compiled from Sul06 (lower-left panel). When more than one possible classification for each CIG galaxy is available in the compilation of Sul06, we adopted the type closer to our results.

Out from 35 galaxies in common with HyperLeda, 37% have  $\Delta T = 0$  and up to 69% have  $|\Delta T| < 2$ . Still one third more show slightly larger morphological differences that appear biased towards small positive differences. This reflects the uniformity in the classification data provided in HyperLeda. However, from 35 galaxies in common with NED, 51% have  $\Delta T = 0$  and up to 77% of the sample have  $|\Delta T| < 2$ . The scatter have significantly narrowed, and this time NED appears to contain more

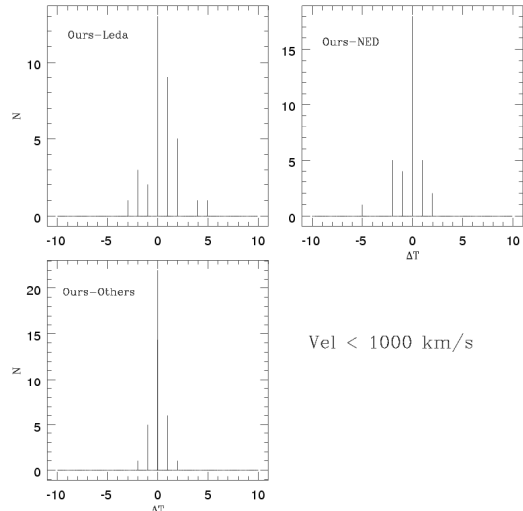


FIG. 9.— Histograms of morphological type differences  $\Delta T = T_{ours} - T_{other}$  for galaxies with  $V < 1000$ . Upper left panel: this work - Leda, right panel: this work - NED and lower panel: this work - other sources. Other sources include individual observations of diverse nature (photographic, photoelectric and CCD) from different authors.

detailed morphological information for nearby objects, contrary to the situation for  $V_r > 1000 \text{ km s}^{-1}$ , probably suggesting a more inhomogeneous nature of the compiled data in that database. Finally, the lower panel of Figure 9 shows that from 35 galaxies in common with other authors, 63% have  $\Delta T = 0$  and up to 94% of them have  $|\Delta T| < 2$ , indicating a significant agreement with our derived types. This is not surprising since nearby galaxies are subject to a more precise morphological classification either from high quality photographic or CCD data.

## 5.2. Bars in isolated S galaxies

Our images show that bars in CIG galaxies come into a variety of sizes, shapes and color distributions; from apparently strong to small ones confined to the central parts of galaxies and up to the oval-shaped bulges, suggesting a range of strengths, lengths, and mass distributions. The tentative fraction of bars found here for the isolated S galaxies with inclination  $i \leq 60^\circ$  is 66.8% (SB=35% and SAB=30.8%); by relaxing the inclination condition, the resultant fraction is about 59%.

As Barazza, Jogee & Marinova (2008) remark, the analyzed galaxy samples in previous works used to be small in number and dominated by early-type spirals. Besides, these samples are for galaxies in any environment, mostly from the field, but not selected to be isolated. The reported fractions of barred disk galaxies in the literature (in the optical) amounts to  $\sim 45\%$ , while in the near-infrared, the fractions seem to increase up to  $\sim 60\%$  (see e.g., Eskridge et al. 2000; Marinova & Jogee 2007, and more references therein). For the large sample of local SDSS disk galaxies analyzed recently by Barazza et al. (2008), the fraction of *large-scale* bars in the *r* band is  $\sim 48\% - 52\%$ . This fraction is smaller than the one reported here. However, we should have in mind that (1) in Barazza et al. 2008 only large-scale bars were considered, a condition that we did not impose, and (2) our bar analysis is based on visual inspections rather than on

quantitative measurements; only a small fraction of spirals (mainly Sa types) were properly judged for the presence of a bar through a deeper analysis of the isophotal ellipticity and  $PA$  profiles. Thus, it might be that our bar fraction in the  $r$ -band is overestimated with respect to Barazza et al. On the other hand, we emphasize that the observed fraction of bars (and rings) in the present paper can hardly be a bias of object selection since we simply gathered galaxies according to their availability on the SDSS database.

If confirmed our finding of about a 65% fraction of bars in the isolated S galaxies ( $r$  band), it would imply that interactions and the global effects of the dense environment are not crucial for the formation of bars, if any, the opposite applies, i.e. the bars tend to be thickened or destroyed more efficiently in the higher density media. The bar thickening or destruction is thought to be at the origin of the boxy/peanut bulges or pseudobulges, and recent simulations in the context of the  $\Lambda$ CDM cosmology show the viability of this proposal (e.g., Avila-Reese et al. 2005; Athanassoula 2005; Bornaud, Combes & Semelin 2005; Martinez-Valpuesta, Shlosman & Heller 2006). It could be that in the bar phenomenon dominate the internal disk galaxy processes rather than the environmental influence (see for a related discussion Hernández-Toledo et al. 2007).

As in previous works, we also found here that the bar occurrence is similar in early- and late-type spirals (c.f. Eskridge et al. 2000; Hernández-Toledo et al. 2007 but see Barazza et al. 2008). What the latter authors report actually is a clear tendency to increase the bar fraction as the  $r_e/R_{24}$  ratio increases ( $r_e$  and  $R_{24}$  are the effective and optical radius, respectively, and their ratio can be interpreted as a measure of the light concentration, and therefore of the bulge-to-disk ratio). For our sample, we have measured the  $C_{80/20}$  concentration, and we confirm that indeed the fraction of barred galaxies significantly depends on it: for  $C_{80/20} \leq 2.5$ ,  $2.5 < C_{80/20} < 3.5$ , and  $C_{80/20} \geq 3.5$  the fraction of barred galaxies increases from  $\approx 55\%$  to  $\approx 63\%$  and  $\approx 78\%$ , respectively. Therefore, we can conclude that while the fraction of barred galaxies does not depend on the morphological type, it does as a function of the light concentration parameter. It is definitively crucial to carry out a deeper study to infer the fraction of bars in samples like the CIG one by using reliable and homogeneously applied bar-detecting techniques.

### 5.3. Morphological distortions in the isolated E galaxies

The morphological properties of nearby E and S0 galaxies in different environments reveal important clues for understanding the nature of their formation. The detection of fine structures, dust lanes, blue cores, and nuclear disks in early-type galaxies, considered evidence of recent merging/accretion events (e.g., Malin & Carter 1983; Lauer 1985; Abraham et al. 1999; Menanteau et al. 2001; Papovich et al. 2003; Lauer et al. 2005; van Dokkum 2005; Bell et al. 2006), tend to occur more frequently in galaxies in the field than in cluster members (Schweizer 1992; Reduzzi et al. 1996; Kuntschner et al. 2002). On the other hand, while the bulk of the stars in luminous cluster E galaxies are old ( $z > 2$ ) and coeval (e.g., Bender et al. 1997; Heavens et al. 2004), in

low-density environments the colors and color gradients of E galaxies suggest that recent bursts of SF occurred (Menanteau et al. 2001, 2005; Stanford et al. 2004; Treu et al. 2005). Blue clumps in early-type galaxies have also been suggested as being evidence of recent accretion episodes (Elmegreen et al. 2005; Pasquali et al. 2006). According to these authors, the fraction of early-type galaxies with blue clumps increases at high redshift.

A long-standing problem of galaxy formation models is related to the existence and the properties of E galaxies in the field. Within the context of the hierarchical CDM model, the natural prediction is that the stars in field luminous E galaxies should be younger on average than those in cluster luminous E galaxies (by  $\approx 4$  Gyr, according to models by Kauffmann 1996). In other words, an isolated luminous E galaxy is expected to assemble late, while its cluster counterpart, assembles early in an overdense region and then its evolution is frozen after this region becomes a dynamically relaxed system (the probability of mergers falls drastically and the mass accretion is even reversed due to tidal stripping and intracluster medium ram pressure). Observational studies show that the stellar populations of field luminous E galaxies are indeed younger than those of cluster E's. However, according to most of the studies, the age differences are small (e.g., Treu et al. 2005; Bernardi et al. 2006; van Dokkum & van der Marel 2007) or intermediate (up to 2 Gyr, e.g., Thomas et al. 2005; Clemens et al. 2006), but not as large as 4 Gyr. Besides, according to Treu et al. (2005), the SF history in the field E's depends strongly on luminosity: the most luminous E's have old stellar populations, while the less luminous ones, show evidence of a significant fraction of stellar mass formed relatively recently. The color-magnitude diagrams as a function of type and local density in Park et al. (2007) show a slight shift of the early-type sequence toward blue color when the local density changes by about an order of magnitude, consistent with the above statements.

The tension between models and observations is reduced significantly when possible effects of AGN feedback are introduced (de Lucia et al. 2006). Nevertheless, still remains the question whether the “dynamical” assembling of field E's was recent or not. The de Lucia et al. (2006) model predicts that massive isolated E's assembled typically 50% of their final mass at  $z < 0.8$ ; such a process is expected to be driven mainly by dry mergers: major mergers between early-type galaxies without the presence of gas. From the observational point of view, it was not an easy task to find pieces of evidence of dry mergers since they progress rapidly, and (i) the post-merger distortions tend to disperse quickly and (ii) they are not in general of easy detection. Massive and detailed morphological studies of early-type galaxies in the field are necessary.

In this work we were able to carry out a detailed morphological study of the isolated CIG $\cap$ SDSS sample. Most of E galaxies in this sample show actually fine structures (e.g., shells, rings, ripples), dust lanes, “diffuse haloes”, and inner disks, as well as disky or boxy isophotes. The finding of these morphological distortions is based on the judgment of the images after different kernel sizes were used in the filtering process of E/S0 galaxies as explained in §3.1 Notice that we did not applied a quantitative procedure for determining dis-

TABLE 6  
ISOPHOTAL SHAPE, FINE STRUCTURE, DUST LANES AND OTHER INTERNAL  
FEATURES IN ISOLATED ELLIPTICALS. *DH* REMAINS FOR A DIFFUSE HALO  
COMPONENT OBSERVED IN SOME ISOLATED ELLIPTICALS.

CIG	boxy/disky	fine structure	dust lanes	inner disks	knots	<i>DH</i>	$g-i$	$M_r$
CIG0189	boxy			disk	knot		1.16	-20.58
CIG0245		shell/ring		disk		<i>DH</i>	1.11	-19.73
CIG0264	boxy			disk	knot	<i>DH</i>	0.98	-21.24
CIG0305		shell?				<i>DH</i>	1.16	-20.64
CIG0396							1.11	-19.97
CIG0437	disky						1.26	-21.76
CIG0513	boxy	ripple?			knot	<i>DH</i>	1.14	-21.77
CIG0517	boxy				knot	<i>DH</i>	1.19	-21.65
CIG0533	boxy	ripple?				<i>DH</i>	1.18	-22.74
CIG0556	disky	ripple?					1.02	-16.73
CIG0557	disky	shell		disk			1.24	-22.31
CIG0578	disky					<i>DH</i>	1.20	-21.43
CIG0582	boxy		dust		knot		1.25	-21.42
CIG0599	disky	shell/ring					1.12	-22.44
CIG0705	disky	shell/ring		disk			1.1	-22.35
CIG0722	boxy						1.18	-22.64
CIG0732	boxy		dust	disk?			1.18	-22.01
CIG0768	disky	shell/ring	dust	disk			0.91	-20.84

tortions with respect to a model light distribution (e.g., Colbert et al. 2001; van Dokkum 2005). The distortions that we call “diffuse haloes” (DH) consist of faint diffuse envelopes that appear symmetric in shape. It is not clear at this moment what is the nature of this component. CIG 533 is an E galaxy showing such a diffuse component. Interestingly CIG 533 is the most luminous galaxy ( $M_r = -22.74$ ) in our list. Notice however that the presence of a nearby (projected on the sky) dwarf galaxy, makes CIG 533 to appear in the list of possible interacting galaxies by Sul06. It should be mentioned that extended luminous halos were found in numerical simulations of galaxy formation in the cosmological context; these faint structures consist of stars shed by merging subunits during the many accretion events that characterize the hierarchical assembly of galaxies (Abadi, Navarro & Steinmetz 2006).

An E galaxy was considered to be boxy or diskly if the  $A_4$  parameter amplitude reached at least a  $\pm 2.5\%$  level within the observed radius. This is a first order estimate and it should be noticed that no normalization to a characteristic radius (e.g., the effective radius,  $r_e$ ) is reported. Examples of boxy and diskly isophotes can be seen in CIG 264 and CIG 768, respectively. In CIG 245 a shell can be appreciated and in CIG 582, dust lanes. In this last case the dust lane appears to affect the fourth-order cosine profile. A localized knot near the central region can also be appreciated. These features together suggest evidence in favor of a merger event.

According to our morphological reevaluation, in the CIG $\cap$ SDSS sample only 3.5% of the galaxies are of E type, showing that the formation of E galaxies in low-density environments is a rare process. The average  $r$ -band luminosity of the E galaxies  $< -21.24 \pm 1.43 >$  confirm the scarcity of luminous E galaxies in isolated environments (e.g., Park et al. 2007). Table 6 lists the E galaxies in this work and their distorted morphology properties. Column (1) gives the CIG number, Column (2) indicates the boxy/disky nature, Column (3) indicates the presence of fine structure in the

form shells/ripples or rings, Column (4) indicates the presence of dust lanes, Column (5) the presence of inner disks, Column (6) the presence blue/red knots, Column (7) the presence of a diffuse halo *DH*, Column (8) gives the  $(g-i)$  color and Column (9) give the  $r$ -band absolute magnitude ( $H_0 = 70 \text{ km s}^{-1} \text{ Mpc}^{-1}$ ). Out of the 18 E CIG $\cap$ SDSS galaxies, at least 15 (83%) are characterized by some kind of morphological distortion: 50% show fine structures, 17% present dust lane structures, 39% show a kind of diffuse halo, and 39% present evidence of an inner disk; in most of the cases a given galaxy presents combinations of several of these distortions. On the other hand, we do not find for most of these E galaxies evidence of blue clumpy tidal tails, which are typical in S-S interactions, as well as of other kind of “smooth” faint tidal features. It is possible that in deeper images, the latter features could appear (see van Dokkum 2005), so that the 83% of E galaxies with morphological distortions found here is actually a lower limit. Notice in Table 6 the incidence of diffuse haloes (*DH*) in some of the E galaxies. We are not clear at this moment about the nature of this component or about its relationship to a merger event.

On the other hand, we have found that among the 18 E galaxies, 8 are boxy and 7 diskly. Interesting enough, among the 4 galaxies with blue colors (tentatively  $g-i < 1.0$ , see Fig. 7), 3 are diskly, and the other one is boxy, but it shows evidence of an inner disk.

According to simulation results, E-E (dry) mergers do not develop prominent clumpy tidal tails and instead are characterized by off-center outer envelopes and the ejections of stars (e.g., Combes et al. 1995), which can be seen as fans, shells, rings, envelopes, and tidal features. This and other works suggest that the perturbation features in the E-E mergers are of short duration (less than 0.5 Gyr), so that their detection implies that the merger happened relatively recently. We look for the presence of  $m = 1$  asymmetries from a Fourier analysis and found no significant amplitudes for the 18 E galaxies in this study.

The numerical simulations also show that the outcome

of merging early-type galaxies is an anisotropic, slowly rotating, boxy spheroid (Naab et al. 2006), while low-mass, highly rotating, disk spheroids are produced typically in unequal-mass spiral mergers (Naab et al. 1999; Naab & Burkert 2003). In general, in order that an E system forms from S-S mergers, the merger should be major (approximate mass ratios in the range 1:1–3:1; e.g., Bournaud, Jog & Combes 2005, and more references therein). The latter authors have found that in the case of intermediate mergers, with mass ratios in the range 4:1–10:1, hybrid systems that could be considered as candidates for S0 galaxies form. In the case of minor mergers, the simulations show that the disturbed disks survive (e.g., Velazquez & White 1999).

In conclusion, we can speculate that most of the isolated E galaxies analyzed here suffered recent major mergers, mostly dry. However, for a few galaxies we find also pieces of evidence of intense knots, central blue colors, in which case a major merger could be expected to have involved at least one disk galaxy. Findings of late SF in isolated E galaxies were also reported by other authors (Treu et al. 2005; Reda et al. 2007). For example, Reda et al. (2007) estimated the age of the stellar populations of a sample of local isolated E’s revealing that several galaxies have central young stars, which also require a recent gaseous accretion or merger. They conclude that a formation scenario of a single dissipative collapse can not explain the spatial distribution of the stellar population and kinematic properties of their studied E isolated galaxies. The main question is now in the statistics: what fraction of isolated E’s show evidence of recent “dynamical” evolution by dry major mergers and what fraction corresponds to E’s with recent SF, product of mergers of galaxies with gas and/or late gas accretion. For the small sample studied here, the former seems to be the case. The above question is relevant for the models of galaxy formation and evolution. Studies with larger samples are needed.

While there is significant evidence that E galaxies could be formed by merging scenarios, the origins of S0 galaxies are more obscure. Since most S0 studies have concentrated on cluster S0 galaxies, the proposed origins of these systems mostly involve processes that remove gas from disk galaxies and thus truncate SF (Mihos et al. 1995; Quilis et al. 2000). However, some of these processes may not be relevant to the histories of very isolated S0 galaxies. The relative numbers of E and S0 galaxies in the CfA survey is 1:4 in favor of S0 galaxies (Marzke et al. 1994). This is in contrast to their relative abundance in the CIG Catalog, 1:1.15 (Sul06) and 1:1.85 (this work), suggesting this the importance of the environment on the formation of S0 galaxies. A possible way to form S0’s in an isolated environment has been mentioned already above: galaxy mergers of intermediate mass ratios, 4:1–10:1 (Bournaud et al. 2005).

#### 5.4. Physical Morphology

We start by exploring how the *CAS* parameters for CIG galaxies do change with wavelength. Figure 10 shows the cumulative distribution function of the *CAS* parameters at *u*, *r* and *z* bands. Significant changes in the *CAS* parameters with wavelength are appreciated. The concentration *C* becomes higher from bluer to redder bands while in the case of both the asymmetry *A* and

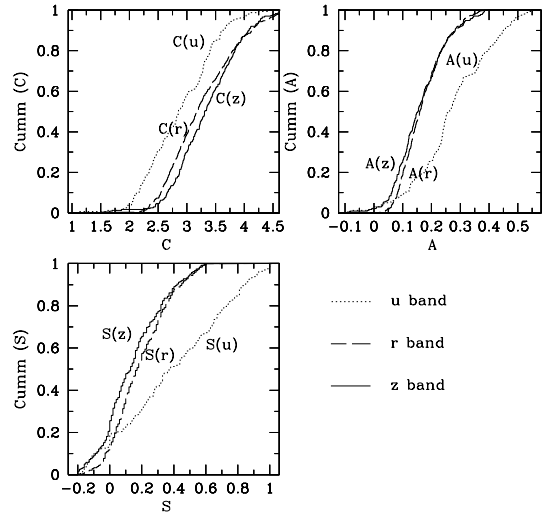


FIG. 10.— Cumulative distribution function of the *CAS* parameters for CIG galaxies at *u*, *r* and *z* bands.

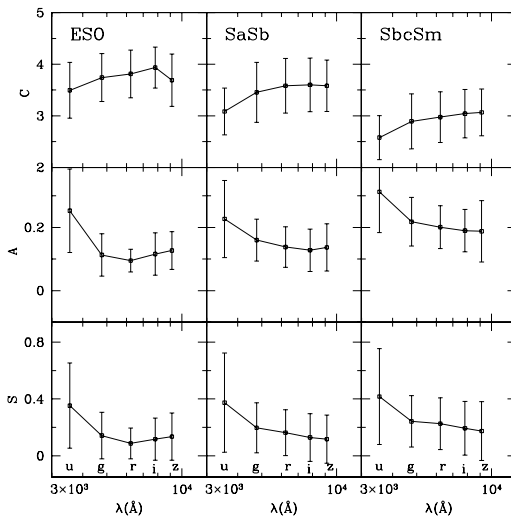


FIG. 11.— Average and standard deviation values of the *CAS* parameters vs SDSS band for CIG galaxies sorted in to E/S0 types (left panel), SaSb types (middle panel) and SbcSm types (right panel).

clumpiness *S* parameters, their values strongly decrease from bluer to redder bands.

In Figure 11 we plot the average and standard deviation values of the *CAS* parameters vs wavelength (color band) for the CIG galaxies sorted into E/S0, early- and late-type spirals (E/S0 –left panel– SaSb –middle panel– and SbcSm –right panel, respectively). The *CAS* parameters of later types show on average more dependence with wavelength than the early types, as well as more scatter at a given band. Among the *CAS* parameters, the clumpiness is the most sensitive to wavelength, although the corresponding error bars indicate a significant dispersion in this parameter.

Figure 12 shows the loci of the CIG∩SDSS galaxies sorted into E/S0, SaSb and SbcSm galaxies in the projected planes of the *r*–band *CAS* space. For comparison, the averages and standard deviations of SaSb and SbcSm

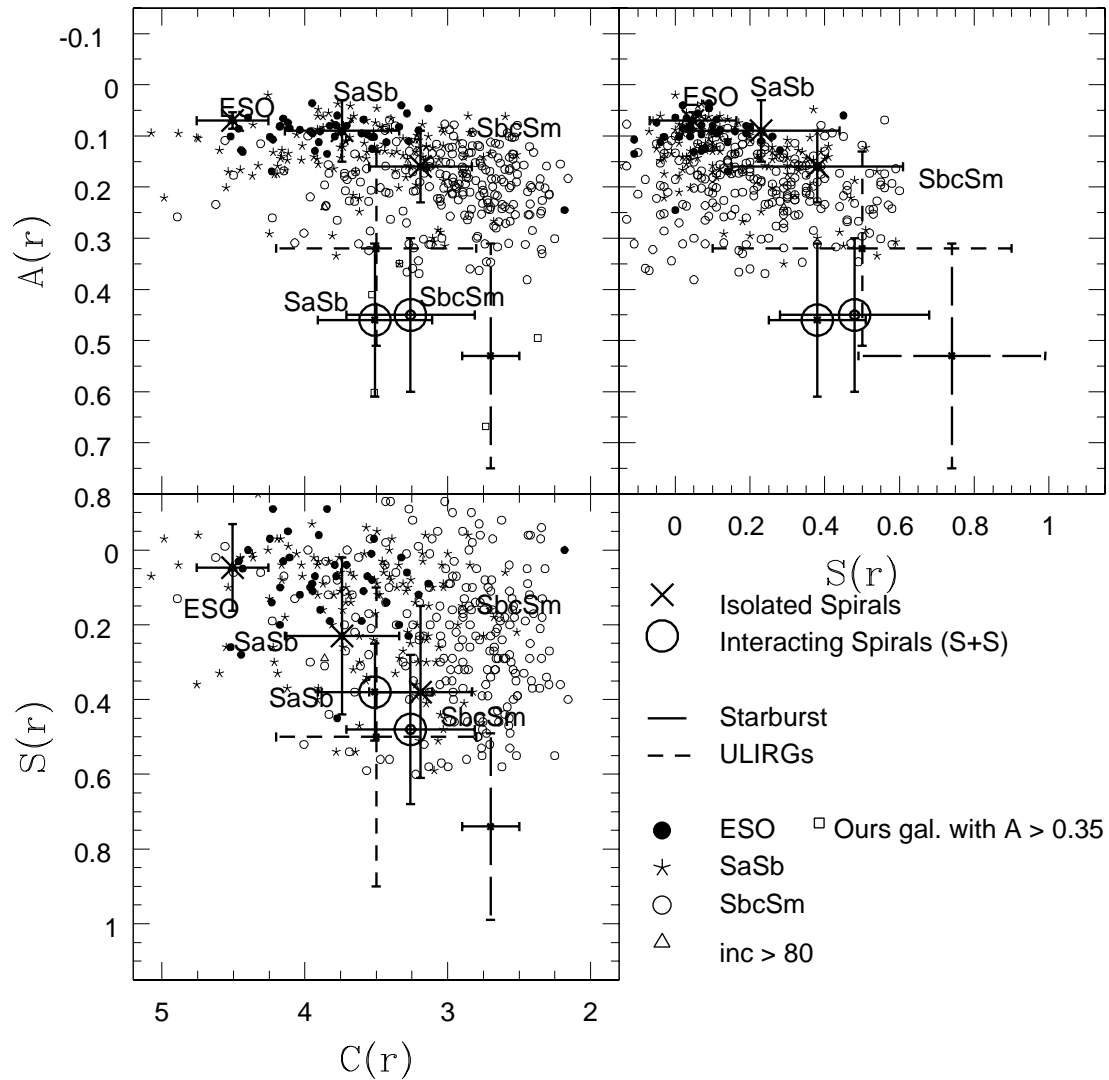


FIG. 12.— The loci of the  $CIG \cap SDSS$  sample in the  $CAS$  diagrams. For comparison, the averages and standard deviations of SaSb and SbcSm subsamples of CIG galaxies in the Johnson-Cousins  $R$ -band system (Hernández-Toledo et al. 2007; 2008) and of E/S0 isolated galaxies from the HyperLeda database (Hernández-Toledo et al. 2006) are shown (crosses and continuous error bars). The  $R$ -band averages and standard deviations of galaxies in interacting S+S pairs (Hernández-Toledo et al. 2005), and Starburst and Ultra Luminous Infrared (ULIR) galaxies (C2003) are also plotted.

subsamples of CIG galaxies in the Johnson-Cousins  $R$ -band system (Hernández-Toledo et al. 2007; 2008) and of E/S0 isolated galaxies from the HyperLeda database (Hernández-Toledo et al. 2006) are shown (crosses and continuous error bars). Also the  $R$ -band averages and standard deviations of galaxies in interacting S+S pairs (Hernández-Toledo et al. 2005), and Starburst and Ultra Luminous Infrared (ULIR) galaxies (C2003) are also plotted.

The question of whether the disk of a galaxy is intrinsically asymmetric or not is of great interest. Some studies have shown that important deviations from axisymmetry exist in the optical and other wavelengths (Rix & Zaritsky 1995; Richter & Sancisi 1994; C2003). However, systematic attempts to quantify asymmetry and other measures like the  $CAS$  parameters in several wavelengths for well-selected local samples of isolated galaxies are rare and missing in the literature.

The asymmetry parameter  $A$  has been shown to be sensitive mainly to galaxy interactions/mergers, but also is influenced by SF clumps, dust lanes, and projection effects. The quantitative measure of  $A$  in the present sample of  $CIG \cap SDSS$  galaxies spans roughly the range  $0.0 \leq A(r) \leq 0.4$ , the average and standard deviation being  $\langle A(r) \rangle = 0.17 \pm 0.07$ . The later types are slightly more asymmetric on average than the earlier ones. The mean asymmetries reported here are definitively lower than the typical ones of interacting disk galaxies (Hernández-Toledo et al. 2005).

Next, we illustrate how the  $CAS$  parameters of the CIG galaxies correlate with other properties and whether these correlations are sensitive to the passband or not. Figure 13 shows the  $griz$  band  $CAS$  parameters vs morphological type  $T$ . Code numbers for each morphological type are now associated according to the HyperLeda convention. The trend seen of the  $CAS$  parameters is a

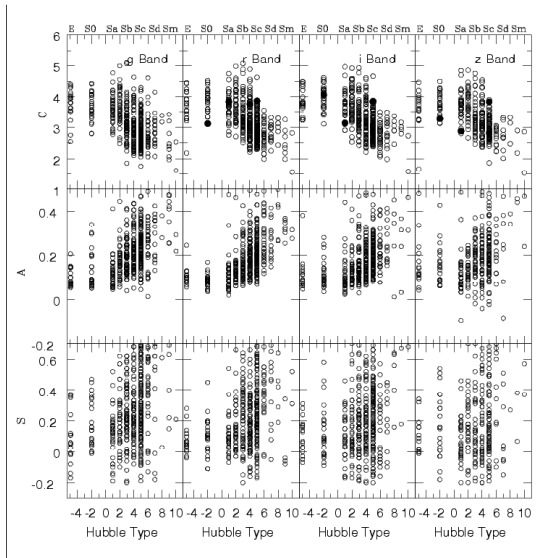


FIG. 13.— The structural  $CAS$  parameters vs the Hubble type for the CIG sample sorted into SDSS band. First column:  $g$ -band, second column:  $r$ -band, third column:  $i$ -band and fourth column:  $z$ -band.

consequence of the natural flocculency and SF in galaxies as they get later in type. SF is more active for later types (as is evidenced also by the trend of higher  $A$  and  $S$  values as the types are later and the color bluer).

The correlations of the  $CAS$  parameters with  $T$  are very scattered, the tightest being with the concentration parameter  $C$  in the sense of smaller values of  $C$  as the type is later. For the  $A$  parameter, one sees only a weak trend of  $A$  on average being higher as the type is latter, and for the  $S$  parameter, it is not possible to define even a trend. The trends of  $C$  and  $A$  with  $T$  are more robust in the  $r$  and  $i$  bands, suggesting this that the basic structure of galaxies is better revealed in the infrared bands.

Figures 14 and 15 show the  $CAS$  parameters vs the total  $(g-i)$  color for the CIG sample sorted into E/S0 and Sa-Sm types, respectively. Corrected colors are presented for Sa-Sm types. Nearly edge-on galaxies (inclination  $\geq 80^\circ$ ) are plotted with crosses. Given that  $A$  and  $S$  are particularly sensitive to projection effects, it is important to visualize these galaxies since they may be masking any trend.

Figure 14 shows the natural scatter in the  $CAS$  parameters and a segregation in blue and red colors for the isolated E/S0 galaxies (Hernández-Toledo et al. 2006). Figure 15 shows the higher sensitivity of the  $CAS$  parameters to intrinsic color variations in isolated spiral galaxies (Hernández-Toledo et al. 2005).

Although it is expected that the color trends are more robust towards the redder bands which are less contaminated from (transient) SF effects thus better representing the basic structure of galaxies, we find a large scatter in the  $z$  band. This is indicating the intrinsically noisier nature of this band.

## 6. SUMMARY AND CONCLUSIONS

The building up of a well-defined sample of local isolated galaxies with uniformly-derived and detailed morphological information is of great relevance because it provides a fair database for comparison with model predictions as well as with observed samples of galaxies in

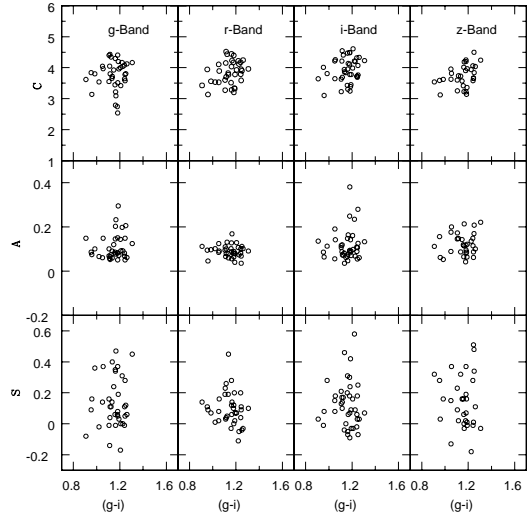


FIG. 14.— The structural  $CAS$  parameters vs the  $(g-i)$  color for E/S0 CIG galaxies, sorted into SDSS band. First column:  $g$ -band, second column:  $r$ -band, third column:  $i$ -band and fourth column:  $z$ -band.

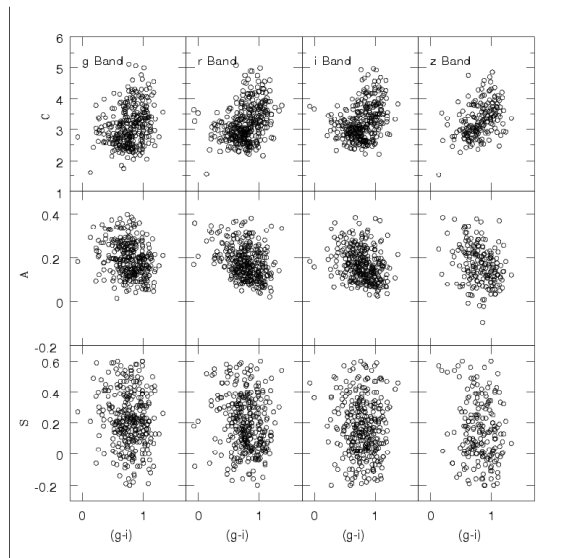


FIG. 15.— The structural  $CAS$  parameters vs the  $(g-i)$  color for SaSm CIG galaxies. Same as in Figure 14.

other environments and at higher redshifts. In this paper we reported (i) a detailed morphological reevaluation of a sample of 549 CIG galaxies that were available in the SDSS(DR6) database, (ii) looked for morphological distortions in the analyzed isolated galaxies, (iii) calculated corrected magnitudes and colors, as well as the structural  $CAS$  parameters for all the galaxies, and (iv) discussed some preliminary conclusions based on the obtained results.

We have taken advantage of the improved scale and dynamic range of the SDSS database and proposed an image processing scheme that enhances the detection of low/high surface brightness morphological and structural components in these CIG galaxies. We have used logarithmic scaled images to look for internal/external details;  $g$  band filtered-enhanced images to look for internal structure in the form of star forming regions, bars,

rings and/or structure embedded into dusty regions; and used complementary RGB color images from the SDSS database to visualize the spatial distribution of the SF and other components like dust (blue colors for recent SF and red colors for older populations/dusty components).

In the case of E/S0/Sa galaxy candidates, we have estimated and used additional information in the form of a surface brightness profile and the corresponding geometric profiles (ellipticity  $\epsilon$ , Position Angle  $PA$  and  $A_4/B_4$  coefficients of the Fourier series expansions of deviations of a pure ellipse) from the  $r$  band images in order to provide evidence of boxiness/diskiness and other structural details that help to discriminate morphology in these galaxies.

The main results and conclusions of the paper are as follow:

–The median morphological type in the present CIG $\cap$ SDSS sample is Sbc ( $T = 4$ ); 35% of the galaxies are earlier than Sbc, and 65% are Sbc or later. This new reevaluation gives somewhat different morphological fractions with respect to previous reports, mainly in the E, S0, Sa and Sab types. While Sul06 found 5.7% of E types, 6.6% of S0 types and 1.4% of transition E/S0 types, amounting to 13.7% of E/S0 galaxies, our results indicate 3.5% of E types and 5% of S0 types, amounting to a fraction of only 8.5% of E/S0 galaxies. This emphasizes the difficulty of finding E/S0 galaxies in environments typical to the isolated galaxies. For early-type S galaxies, while Sul06 found 1.3% of Sa types and 5.1% of Sab types, we accounted for 6.5% of Sa types and 7.8% of Sab types. In general, for 74% of the galaxies in common with Sul06 both classifications have a difference  $|\Delta T| < 2$ .

–For the 539 CIG $\cap$ SDSS galaxies we have calculated the absolute magnitudes in the bands  $gri$  and corrected by both the Galaxy and internal extinction. The average and  $1\sigma$  dispersions of the  $g-i$  color for the E/S0, Sa–Sb, and Sbc–Sm/Irr morphology ranges are  $1.18 \pm 0.26$ ,  $0.89 \pm 0.21$ , and  $0.66 \pm 0.55$ , respectively. The color–magnitude diagram for the E/S0’s is quite flat and narrow, while for the disk galaxies, a trend of redder galaxies as they get brighter, but with a large scatter is appreciated.

–We reported a tentative  $r$ –band fraction of bars in disk galaxies of 65.8% (defined only by an eye inspection and excluding objects with  $i > 60^\circ$ ); 35% are clearly barred (SB), and 30.8% show evidence of a weak bar (SAB). The reported fraction of bars in the present CIG isolated disk galaxies is larger than others reported in the literature for samples related to field and cluster/group environments. The fraction of barred galaxies does not change with the morphological type, but it correlates significantly with the light concentration parameter  $C_{80/20}$ . We have also found 33.3% of the disk galaxies showing ring structures.

–Our image processing scheme of the SDSS data allowed us to find a richness of distinct substructure in the isophotal shapes of the E galaxies as well as a series of morphological distortions. Out of the 18 E galaxies in the sample, 8 (44%) show boxy isophotes and 7 (38%) show disk isophotes. Among the 4 blue E’s ( $g-i < 1$ ), 3 are disk and 1 boxy, but the latter shows evidence of an inner disk. The fraction of E’s with one or more kinds of morphological distortion amounts to 78%: fine

structures (50%), dust lane structures (17%), diffuse halo (39%), and inner disk (39%). Our results suggest that most of the isolated E’s suffered recent dry major mergers (E–E). Only a few of them show pieces of evidence of mergers of galaxies with gas, and/or of late gas accretion and intense SF.

–In order to complement our morphological study, we have estimated the  $ugriz$  band  $CAS$  parameters of the 549 CIG $\cap$ SDSS galaxies as part of a model-independent morphological system. The  $CAS$  averages and standard deviations in the  $r$ –band for the E/S0 galaxies are  $\langle C \rangle = 3.81 \pm 0.46$ ,  $\langle A \rangle = 0.09 \pm 0.03$ ,  $\langle S \rangle = 0.08 \pm 0.10$ , for the SaSb galaxies are  $\langle C \rangle = 3.58 \pm 0.52$ ,  $\langle A \rangle = 0.14 \pm 0.06$ ,  $\langle S \rangle = 0.16 \pm 0.16$ , and for the SbcSm galaxies are  $\langle C \rangle = 2.97 \pm 0.49$ ,  $\langle A \rangle = 0.20 \pm 0.07$ ,  $\langle S \rangle = 0.25 \pm 0.18$ . These values are in rough agreement with those reported previously for smaller samples of isolated galaxies in the  $R$ –band Johnson-Cousins system (Hernández-Toledo et al. 2006;2008). The mean asymmetries reported here are definitively lower than the typical ones for interacting disk galaxies (Hernández-Toledo et al. 2005). While the  $C$  parameter systematically increases from bluer to redder bands, both  $A$  and  $S$  significantly decrease. The  $CAS$  parameters present more robust trends with the morphological type  $T$  and the total ( $u-r$ ) color in the redder bands, suggesting that the basic structure of galaxies is revealed better in the redder bands. In any case, the mentioned trends are very noisy, the less scattered being with  $C$ .

H.M.H.T. thanks the staff of the Observatorio Astronómico Nacional in San Pedro Mártir, B. C. for the help in the observations of subsamples of the CIG in the Johnson-Cousins photometric system. The authors thank Changbom Park for fruitful discussions. This work was funded by CONACYT grant 42810 to H.M.H.T., J.A.V.M. and S.O.E. We thank referee Michael S. Vogeley for his comments/suggestions that improved the content of this manuscript.

This research has made use of the NASA/IPAC Extragalactic Database (NED) which is operated by the Jet Propulsion Laboratory, California Institute of Technology, under contract with the National Aeronautics and Space Administration.

We acknowledge the usage of the HyperLeda database (<http://leda.univ-lyon1.fr>).

Funding for the SDSS and SDSS-II has been provided by the Alfred P. Sloan Foundation, the Participating Institutions, the National Science Foundation, the U.S. Department of Energy, the National Aeronautics and Space Administration, the Japanese Monbukagakusho, the Max Planck Society, and the Higher Education Funding Council for England. The SDSS Web Site is <http://www.sdss.org/>.

The SDSS is managed by the Astrophysical Research Consortium for the Participating Institutions. The Participating Institutions are the American Museum of Natural History, Astrophysical Institute Potsdam, University of Basel, University of Cambridge, Case Western Reserve University, University of Chicago, Drexel University, Fermilab, the Institute for Advanced Study, the Japan Participation Group, Johns Hopkins University,

the Joint Institute for Nuclear Astrophysics, the Kavli Institute for Particle Astrophysics and Cosmology, the Korean Scientist Group, the Chinese Academy of Sciences (LAMOST), Los Alamos National Laboratory, the Max-Planck-Institute for Astronomy (MPIA), the Max-

Planck-Institute for Astrophysics (MPA), New Mexico State University, Ohio State University, University of Pittsburgh, University of Portsmouth, Princeton University, the United States Naval Observatory, and the University of Washington.

## REFERENCES

- Abadi, M. G., Navarro, J. F., & Steinmetz, M. 2006, *MNRAS*, 365, 747
- Abraham, R. G., Tanvir, N. R., Santiago, B. X., Ellis, R. S., Glazebrook, K., & van den Bergh, S. 1996, *MNRAS*, 279, L47
- Abraham, R. G., Ellis, R. S., Fabian, A. C., Tanvir, N. R., & Glazebrook, K. 1999, *MNRAS*, 303, 641
- Avila-Reese, V., Colín, P., Gottlöber, S., Firmani, C., & Maulbetsch, C. 2005, *ApJ*, 634, 51
- Avila-Reese, V., Zavala, J., Firmani, C. & Hernández-Toledo, H. M. 2008, *AJ*, in press
- Athanassoula, E. 2005 *MNRAS*, 358, 1477
- Barazza, F. D., Jogee, S., & Marinova, I. 2008 *ApJ*, 675, 1194
- Bell, E. F., et al. 2006, *ApJ*, 640, 241
- Bender, R., 1988, *A&A*, 193L, 7B
- Bender, R., Saglia, R. P., & Ziegler, B. 1997, in *The Early Universe with the VLT*, ed. J. Bergeron et al. (Berlin: Springer), 105
- Bernardi, M., Nichol, R. C., Sheth, R. K., Miller, C. J., & Brinkmann, J. 2006, *AJ*, 131, 1288
- Bershady, M. A., Jangren, A., & Conselice, C. J. 2000, *AJ*, 119, 2645
- Bournaud, F., Jog, C. J., & Combes, F. 2005, *A&A*, 437, 69
- Buta, R. 1995, *ApJS*, 96, 39
- Clemens, M. S., Bressan, A., Nikolic, B., Alexander, P., Annibali, F., & Rampazzo, R. 2006, *MNRAS*, 370, 702
- Colbert, J. W., Mulchaey, J. S., & Zabludoff, A. I. 2001, *AJ*, 121, 808
- Combes, F., Rampazzo, R., Bonfanti, P. P., Pringniel, P., & Sulentic, J. W. 1995, *A&A*, 297, 37
- Conselice, C. J. 1997, *PASP*, 109, 1251
- Conselice, C. J. 2003, *ApJS*, 147, 1 (C2003)
- Conselice, C. J., Bershady, M. A., & Gallagher, J. S., III 2000, *A&A*, 354, L21
- De Lucia, G., Springel, V., White, S., Croton, D., & Kauffmann, G. 2006, *MNRAS*, 366, 499
- Elmegreen, D. E., Elmegreen, B. G., & Ferguson, T. E. 2005, *ApJ*, 623, L71
- Eskridge, P. B., et al. 2000, *AJ*, 119, 536
- Frei, Z., Guhathakurta, P., Gunn, J. E., & Tyson, J. A. 1996, *AJ*, 111, 174.
- Fukugita, M., Ichikawa, T., Gunn, J. E., Doi, M., Shimasaku, K. & Schneider, D. P. 1996, *AJ*, 111, 1748F
- Gott, J. R., & Thuan, T. X. 1976, *ApJ*, 204, 649
- Gunn, J. E., Carr, M., Rockosi, C., et al. 1998, *AJ*, 116, 3040G
- Heavens, A., Panter, B., Jimenez, R., & Dunlop, J. 2004, *Nature*, 428, 625
- Hernández-Toledo, H. M., Avila-Reese, V., Conselice, C. J., & Puerari, I. 2005, *AJ*, 129, 682
- Hernández-Toledo, H. M., Avila-Reese, V., Salazar-Contreras, J. R., & Conselice, C. J. 2006, *AJ*, 132, 71
- Hernández-Toledo, H. M., Zendejas-Domínguez, J., Avila-Reese, V. 2007 *AJ*, 134, 2286
- Hernández-Toledo, H. M., & Ortega-Esbrí, S. 2008, *A&A*, submitted
- Hogg, D. W., Finkbeiner, D. P., Schlegel, D. J. & Gunn, J. E. 2001, *AJ*, 122, 2129
- Hoyle, F., Rojas, R. R., Vogeley, M. S., Brinkmann, J. 2005, *ApJ*, 620, 618.
- Karachentseva, V. E. 1973, *Astrof. Issledovanija Byu. Spec. Ast. Obs.*, 8, 3
- Kauffmann, G., 1996, *MNRAS*, 281, 487
- Kuntschner, H., Smith, R. J., Colless, M., Davies, R. L., Kaldare, R., Vazdekis, A. 2002, *MNRAS*, 337, 172
- Lauer, T. R., 1985, *MNRAS*, 216, 429
- Lauer, T. R., et al. 2005, *AJ*, 129, 2138
- Lupton, R. H., Ivezić, Z., Gunn, J. E., Knapp, G., Strauss, M. A., Yasuda, N. 2002, *SPIE*, 4836, 350L
- Malin, D. F., & Carter, D. 1983, *ApJ*, 274, 534
- Marinova, I., & Jogee, S. 2007, *ApJ*, 659, 1176
- Martínez-Valpuesta, I., Shlosman, I., & Heller, C. 2006, *ApJ*, 637, 214
- Marzke, R. O., Huchra, J. P., Geller, M. J., & Corwin, H. G. 1994, *AJ*, 108, 437
- Menanteau, F., Abraham, R. G., & Ellis, R. S. 2001, *MNRAS*, 322, 1
- Menanteau, F., et al. 2005, *ApJ*, 620, 697
- Mighell, K. J. 1999, *ASPC*, 172, 317M
- Mihos, J. C. 1995, *ApJ*, 438, L75
- Morgan, W. W., & Osterbrock, D. E. 1969, *AJ*, 74, 515
- Naab, T., & Burkert, A. 2003, *ApJ*, 597, 893
- Naab, T., Burkert, A., & Hernquist, L. 1999, *ApJ*, 523, L133
- Naab, T., Khochfar, S., & Burkert, A. 2006, *ApJ*, 636, L81
- Nieto, J. L., Capaccioli, M. & Held, E. V. 1988, *A&A*, 195L, 1N
- Papovich, C., Gialalisco, M., Dickinson, M., Conselice, C. J., & Ferguson, H. C. 2003, *ApJ*, 598, 827
- Park, Ch., Vogeley, M. S., Geller, M. J., Huchra, J. P. 1994, *ApJ*, 431, 569.
- Park, C., Gott, J. R., & Choi, Y.-Y. 2008, *ApJ*, in press
- Park, C., Gott, J. R., & Choi, Y.-Y. 2008, *ApJ*, in press
- Park, C., Choi, Y.-Y., Vogeley, M. S., Gott, J. R. I., & Blanton, M. R. 2007, *ApJ*, 658, 898
- Pasquali, A., et al. 2006, *ApJ*, 636, 115P
- Patuel G., Petit C., Prugniel P., Theureau G., Rousseau J., Brouty M., Dubois P., Cambrésy L., 2003, *A&A*, 412, 45
- Quilis, V., Moore, B., & Bower, R. 2000, *Science*, 288, 1617
- Reda, F. M., Proctor, R. N., Forbes, D. A., Hau, G. K. T., Larsen, S. S. 2007, *MNRAS*, 377, 1772
- Reduzzi, L., Longhetti, M., Rampazzo, R. 1996, *MNRAS* 282, 149 (RLR96)
- Richter, O., & Sancisi, R. *A&A*, 290 L 9
- Rix, H., & Zaritsky, D. *ApJ*, 447, 82
- Saucedo-Morales, J., & Biegging, J. 2001, *APSSS*, 277, 449
- Schlegel, D.J., Finkbeiner, D.P. & Davis, M., 1998, *ApJ*, 500, 525
- Schweizer, F., & Seitzer, P. 1992, *AJ*, 104,1039
- Smith, J. A., et al. 2002, *AJ*, 123, 2121
- Sofue, Y. 1993, *PASP*, 105, 308
- Stanford, S. A., Dickinson, M., Postman, M., Ferguson, H. C., Lucas, R. A., Conselice, C. J., Budavari, T., & Somerville, R. 2004, *AJ*, 127, 131
- Stoughton, C., et al. 2002, *AJ*, 123, 485
- Sulentic, J. W. 1989, *AJ*, 98, 2066
- Sulentic, J. W., Verdes-Montenegro, L., Bergond, G., et al. 2006, *A&A*, 449 937
- Thomas, D., Maraston, C., Bender, R., & Mendes de Oliveira, C. 2005, *ApJ*, 621, 673
- Treu, T., Ellis, R. S., Liao, T. X., & van Dokkum, P. G. 2005, *ApJ*, 622, L5
- Tully, R. B., & Pierce, M. J. 2000, *ApJ*, 533, 744
- Tully, R.B., Pierce, M.J., Huang, J., Saunders, W., Verheijen, M.A.W. & Witchalls, P.L., 1998, *AJ*, 115, 2264
- van Dokkum, P. G. 2005, *AJ*, 130, 2647
- van Dokkum, P. G., & van der Marel, R. P. 2007, *ApJ*, 655, 30
- Velazquez, H., & White, S. D. M. 1999, *MNRAS*, 304, 254
- Verley, S., Leon, S., et al. 2007, *A&A*, 472, 121
- Wozniak et al. 1995, *AAPS*, 111, 115